Long-term magnetic anomalies and its possible relationship to the latest greater Chilean earthquakes in the context of the seismo-electromagnetic theory

Enrique Guillermo Cordaro[1, 2], Patricio Venegas-Aravena[1, 3, 4] and David Laroze[5].

1. Observatorios de Radiación Cósmica y Geomagnetismo, Departamento de Física, F.C.F.M., Universidad de Chile, Casilla 487-3, Santiago, Chile.
2. Facultad de Ingeniería. Universidad Autónoma de Chile. Pedro de Valdivia 425. Santiago, Chile.
3. Department of Structural and Geotechnical Engineering, School of Engineering, Pontificia Universidad Católica de Chile, Vicuña Mackenna 4860, Macul, Santiago, Chile.
4. Research Center for Integrated Disaster Risk Management (CIGIDEN), Santiago, Chile.
5. Instituto de Alta Investigación, Universidad de Tarapacá, Casilla 7D, Arica, Chile.

Abstract

Several magnetic measurements and theoretical development from different research groups have shown certain relationships with worldwide geological processes. Secular variation of geomagnetic cutoff rigidity, magnetic frequencies, or magnetic anomalies have been linked with spatial properties of active convergent tectonic margin or earthquakes occurrences during recent years. These include the rise of similar fundamental frequencies in the range of micro hertz before Maule 2010, Japan 2011, and Sumatra 2004 earthquakes and the dramatic rise of the cumulative number of magnetic anomalous peaks before several earthquakes as Nepal 2015 and Mexico 2017, among others. Currently, all of these measurements have been physically explained by the microcrack generation due uniaxial stress change in rock experiments. The basic physics of these experiments have been used to describe the lithospheric behavior in the context of the seismo-electromagnetic theory. Due to the dramatic increase in experimental evidence, physical mechanism and theoretical framework, this paper analyses vertical magnetic behavior close to the latest three main earthquakes in Chile: Maule 2010 (Mw8.8), Iquique 2014 (Mw8.2), and Illapel 2015 (Mw8.3). The FFT, Wavelet transform and daily cumulative number of anomalies methods were used during quiet space weather time during one year before and after each earthquake in order to filter space influence. FFT Method confirms the rise of power spectral density in the mHz range before one month each earthquake, which decreases to lower values after some months after earthquake occurrence. The cumulative anomalies method exhibited an increase previous to each Chilean earthquake (50-90 days prior earthquakes) similar to those found for Nepal 2015 and Mexico 2017. The wavelet analyses also show as similar properties as FFT analysis. However, the lack of physics-based constraints in the wavelet analysis do not allow conclusions as strong as FFT and cumulative methods. By using these results and previous research, it could be stated that these magnetic features could give seismic information from impending events. Additionally, these results could be related to the Lithosphere-Atmosphere-Ionosphere coupling (LAIC effect) and the growth of microcracks and electrification in rocks described by the seismo-electromagnetic theory.

1. Introduction

As earthquakes are geological events that might cause great destruction, studies about their preparation stage and generation mechanism are a matter of concern. That is why scientific studies offering new information, evidence or insights about different physical mechanisms or activation insights during the seismic cycle, improve our understanding of earthquakes occurrences. Currently, one of the most controversial physical mechanisms that is being studied is the lithospheric electromagnetic variations as earthquake's precursory signals. Nevertheless, the study of magnetic and geological relationships is not something new. For example, the decadal variations of the geomagnetic field have been associated with an irregular flow of the outer core (Prutkin, 2008). Thus, the secular variation of the magnetic field can be interpreted as the response of the movement of the fluid outer core interacting with the topography of the lower mantle. Then, as that topography in the core-mantle boundary corresponds to a projection of the topography of the earth's surface (Soldati et al., 2012), it was not surprising that Cordaro et al. (2018) and Cordaro et al. (2019) found significant variations of geomagnetic cutoff rigidity Rc at relevant geological places in the Chilean margin.

Regarding earthquakes, many attempts to determine the location, date and magnitude of seismic movements have been made in the past (e.g. Jordan et al., 2011), but these historical efforts have failed to conclude that it is possible to use seismological data as a predictive tool (Geller, 1997). Besides, when less classical methods (e.g., electromagnetic methods) have been used since some decades ago. First attempts on this topic can be found in the work of Varotsos - Alexopoulos - Nomicos (VAN) (see Varotsos et al., 1984, and the references therein). Techniques for seismic-electrical signals associated with the VAN method has been considerably improved and applied in several contexts (see Varotsos et al., 2019, and the references therein). Also, some debates about this theory can be found in the work of Hough (2010). Recently, electromagnetic methods have risen with relevant and concluding evidence. Specifically, it is because physical mechanism, based on the Zener-Stroh mechanism, links micro cracks to magnetic anomalies and fault's friction is currently available (e.g., Stroh, 1955, Slifkin, 1993, Venegas-Aravena et al., 2019, Venegas-Aravena et al., 2020), wide frameworks are being studies (holistic interaction between lithosphere, ionosphere and atmosphere, e.g. De Santis et al., 2019, Yu et al., 2021). Moreover, different electromagnetic theories related to earthquakes have been implemented. For example, De Santis et al. (2017) and De Santis et al. (2019b), showed the method of magnetic anomalies in which long-term magnetic data from different satellites (ionosphere level) were considered during quiet or no disturbed periods due to the space weather. After removing a known magnetospheric process from data as daily variation, the remaining magnetic perturbation or anomaly could be considered as lithospherical origin. This method allowed them to study magnetic measurements mostly free of external perturbation prior and after 16 worldwide earthquakes of magnitude approximately greater than Mw 6.5. When satellites covered areas close to each earthquake locations, they found an increase in the number of magnetic anomalies prior (1-3 months) to the occurrence of these earthquakes and a decrease after the earthquake (De Santis et al., 2017, Marchetti and Akhoondzadeh, 2018, Marchetti et al., 2019a, b, De Santis et al., 2019b).

Other methodologies also support certain statistical correlations to earthquake's preparation phase. For instance, the rise of magnetic signals characterized by a wide range of ultra-low frequencies (5-100 mHz and 5.68 – 3.51 μHz) or the ionospheric disturbs before several earthquakes have been widely and intensively reported during a couple of decades (Hayakawa and Molchanov, 2002, Pulinets and Boyarchuk, 2004, Varotsos, 2005, Balasis and Mandea 2007, Foppiano et al., 2008, Molchanov and Hayakawa, 2008, Liu, 2009, Hayakawa et al., 2015, Contoyiannis et al., 2016, Potirakis et al., 2016, Villalobos et al., 2016, De Santis et al., 2017, Oikonomou et al., 2017, Cordaro et al., 2018, Marchetti and Akhoondzadeh, 2018, Potirakis et al., 2018, Ippolito, et al., 2020, Varotsos et al., 2019, Florios, et al., 2020, Pulinets et al., 2021, among others).

The magnetic phenomena not only have risen during decadal or preparation state, but also during the fast coseismic stage. For example, small magnetic variations (~0.8 nT) at ~100 km were measured during the Tohoku 2011 Mw9.0 earthquake (Utada et al., 2011). Similar findings were shown by Johnston et al. (2006) during the Parkfield 2004 Mw6.0 earthquake (~0.3 nT) at ~2.5 km. In addition, peaks of ~0.9 nT were measured at ~7 km during the Loma Prieta 1989 Mw7.1 earthquake (Fenoglio et al., 1995, Karakeliana et al., 2002). The above-mentioned reports have shown strong evidence of the presence of magnetic signals during the seismic preparation stage and during the rupture process itself. Up to this date, there are several experiments and theoretical models that identify and explain the physical mechanism of different magnetic variations related to geological properties (e.g. Freund, 2010, Scoville et al., 2015,

Yamanaka et al., 2016, Venegas-Aravena et al., 2019, Vogel et al. 2020, Yu et al., 2021). According to experiments, the rise of electrical current flux within rocks is due the movement of imperfections and the suddenly growth of microcracks when rock samples are being uniaxially stressed in the semi-brittle regime (Anastasiadis et al., 2004, Stavrakas et al., 2004, Ma et al., 2011, Cartwright-Taylor et al., 2014, among others). The applied external stress generates the internal collapse of rock, which imply the fast growth of microcracks and the increase of electrical currents that flows throughout the crack right before the failure of rock samples (e.g. Triantis et al., 2008, Pasiou and Triantis, 2017, Stavrakas et al., 2019). These currents created by this mechanism are known as pressure stimulated currents (PSC) and its rise occurs mainly when the rock samples abandon linearity (see Triantis et al. (2020) and references therein for further details). This pre-failure indicator has been used as the experimental base for theoretical descriptions of impending earthquakes at lithospheric scale (Tzanis and Vallianatos, 2002, Vallianatos and Tzanis, 2003, Venegas-Aravena et al., 2019, Venegas-Aravena et al., 2020). This seismo-electromagnetic theory has explained the frequency range, the cumulative number of anomalies, the coseismic signals, friction states at fault, and the b-value time evolution by considering fast stress changes in the fault surrounding area. This area of fast stress changes was theorized by Dobrovolsky et al. (1979) and it could cover thousands of kilometers. Similarly, Venegas-Aravena et al. (2019) also found that the growth of microcracks and magnetic signals are hosted by these stress conditions within this large area. Recently, large areas of fast stress and strain changes, that surround the impending earthquakes, has been also confirmed by GPS analysis (Bedford et al., 2020).

Despite the abovementioned evidences, still there are no reports of cumulative anomalies in one the most actives margin: the Chilean margin (e.g., Vigny et al., 2011, Pedrera et al., 2014, Carvajal et al., 2017, Zhang et al., 2017, Abad et al., 2020, Satake et al., 2020). In Figure 1 one can observe the historical strong earthquakes across the Chilean margin. That is why this works present a wide study of magnetic signals which include spectral (Fourier and Wavelet analysis), cumulative, and space weather analysis one year before and after the latest three main megathrust earthquakes in Chile: Maule 2010 (Mw8.8), Iquique 2014 (Mw8.2), and Illapel 2015 (Mw8.3). The space weather and general magnetic conditions are found in Section **2**. The main magnetic and frequency analysis are defined and performed in Section **3**. The relation between results and physical mechanism from the seismo-electromagnetic theory is Section **4**. Finally, discussions and conclusions are in Section **5**.

2. Data processing consideration regarding the space weather and magnetic conditions

In order to perform a clear interpretation of the results, any methods and data processing must answer the classic questions: 1) What is actually being measured? 2) Where do the disturbances come from? 3) How should the disturbing data be removed? Here, the proper way to answer the above-mentioned questions is by the recognition of the physical process, which generates external disturbances on measurements. Then, the uses of the standard index convention that identify disturbed times, and statistical analysis. This led us to implement four filters before working. These filters are:

1.- DST filter: Eliminate periods of high solar magnetic activity. That is, the data within these periods are useless since the terrestrial cannot be distinguished from the solar.

2.- Daytime filter (or quiet time): Eliminate daytime data as they reflect the interaction of the solar wind with the magnetosphere.

3.- Stochastic filter: Moving averages eliminate the low-frequency variations associated with the usual flow of the ionosphere. Experiments and theory show that electrification of rocks prior to failure occurs mainly in the millihertz range (e.g., Triantis et al., 2012). Thus, moving averages filter the lower frequencies by using residuals methods to contain error propagation, that is, the difference between the signal and its smoothed signal.

4.- Recurrence filter: This filter controls the failure of the other 3. Specifically, by means, the definition of anomalous residual implies that any magnetic anomaly must be uncommon. Thus, the probability of finding an anomalous residual within a given period should be tended to zero. In other words, few anomalies should be measured in the period. This indicates that if the number of detected anomalies dramatically increases, they are more common, and thus, not all of them could be considered anomalous. This contradiction could arise in two scenarios: a) if a large number of anomalies occurs during the entire period, it means that the threshold should increase. b) If a large number of anomalies occurs during a short period of time, let say

during one single day out of several months or years, then, it means that filters 1, 2 and 3 were insufficient to filter that specific day which implies that day cannot be considered.

Finally, the resulting filtered variations are potentially generated in the lithosphere, not in the space or ionospheric environment. It is important to note that the remaining data is almost unchanged since the analysis studies the applicable periods. With this added to records of several years, we eliminate one of the most significant scientific community's concerns: the origin of disturbances, propagation of errors, and false positives. After this process, spectrograms or other methods can be used. That is, it requires a very sophisticated preparation to discern and identify problematic disturbances in the records. As this is a sophisticated filter process will be detailed in the following Sections.

2.1 External magnetic disturbances

Before going to the study of the magnetic field and its temporal variations, it should be remembered that the rate of change of the magnetic field is influenced by the rate of variation of the spatial particle count. These are different cases of irregular and regular phenomena of the nearby space climate. Regular magnetic variation creates periodic fluctuations in the interplanetary magnetic field in a wide range of periods, from few day periods up to seasonal variations (Moldwin, 2008, Blagoveshchensky et al., 2018, Yeeram, 2019). Irregular variations occur when sudden increases of incoming solar particles are recorded across the geomagnetic field. This particle disturbance induces a 10% to 20% decrease in magnetic field intensity because of the change in pressure that extraterrestrial particles exert on the magnetosphere, an effect that can last from a couple of hours to several days (Russel et al., 1999). One explication is that particles following the magnetic field lines, in the turbulent magnetic reconnection that is present in the diurnal variation and the regular variations (Priest and Forbes, 2000, Kulsrud, 2004, Cordaro, et al., 2016, Lazarian et al., 2020). Other minor irregular magnetic fields as auroral events and electric current in the ionosphere are not considered for this paper (see Diego et al. (2005) for detailed description for these phenomena).

Some indices are used in order to measure the space disturbances and its manifestation in the geomagnetic field. For example, the Kp index measure the influence of geomagnetic storms in the horizontal magnetic field (Dieminger et al., 1996), while Dst index is interpreted as a measure of the magnetospheric ring-current strength which is proportional to the particle's kinetic energy (e.g. Silva et al., 2017). Usually, Dst index could increase dozens or hundreds of nT during magnetic storms (Kp> 4), that is why it is important to incorporate these indices to create reliable magnetic models.

2.2 Secular variation in the Chilean convergent margin

The magnetic response to these disturbances requires a reference model that allows to discriminate earth's magnetic features from disturbs that spreads throughout interplanetary magnetic fields. One of those features corresponds to the magnetic shielding against incoming turbulent particles which is known as geomagnetic cutoff rigidity Rc (Pomerantz, 1971). The rigidity Rc is defined as the product of the force of the magnetic field and the curvature radius of the incident particle r_g and it can be estimated globally by using the Tsyganenko magnetic field model (for details see: Smart et al., 2000, Smart and Shea, 2001, Tsyganenko, 2002a, 2002b). The Rc variations describes geomagnetic secular variations which could be related to geological features in the Chilean margin (Pomerantz, 1971, Shea and Smart, 2001, Smart and Shea, 2005, Herbst et al., 2013, Cordaro et al., 2018, Cordaro et al., 2019). For example, regarding to latitudinal effect (Pomerantz, 1971), Cordaro et al. (2019) found that the highest variation rate of effective Rc values were obtained at 46.5°S, 76°W and at and at 52°S, 76.5°W (Figure 1). The first one is in the Taitao Peninsula, Chile which corresponds to the triple junction point of three tectonic plates: Nazca, South America, and Antarctica. The second one is close to Puerto Natales in the Strait of Magellan area, also a triple junction point of three tectonic plates: South America, Antarctica and Scotia (Figure 1). There are other geological and geomagnetic links as the flat slab in the Chilean convergent margin (Cordaro et al. 2018, Cordaro et al. 2019). However, these results are not surprising because changes in Rc represent secular variations that represent magnetic secular variations created at the outer core (Bloxham et al., 2002, McFadden and Merrill, 2007, Sarson, 2007, Finlay, 2007, Herbst et al., 2013). Specifically, 3D models of core mantle boundary (CMB) topology based on the velocities of seismic waves (Simmons et al., 2010) show the existence of positive topography in upthrust regions and negative topography in subduction zones (Yoshida, 2008, Lassak et al., 2010, Soldati et al., 2012). Let us remark that the intensity of the geomagnetic

field at within the outer core is estimated to be of the order of 2-4 mT (rms) (Olson et al., 1999, Olson, 2015), while at earth surface varies between 20,000 and 60,000 x 10^{-9} T.

The most relevant magnetic feature in the Chilean sector is the low magnetic intensity values that correspond to the influence of the South Atlantic Magnetic Anomaly (SAMA) (e.g. Cordaro et al., 2016). Recently, Tarduno et al. (2015), argued that SAMA is being created by a topography structure in the CMB beneath south Africa. SAMA is not only linked with global magnetic features as a geomagnetic dipole moment (e.g. Heirtzler, 2002, Gubbins et al., 2006), it is also corresponding to the closer area between earth's surfaces and radiation belt. This proximity allows more charged particles and more disturbances in the magnetic field near the Chilean margin (e.g. Kivelson and Russell, 1995). That is why a proper magnetic response to external disturbances is required before and after earthquakes occurrences.

2.3 Magnetic perturbation during seismic events of 27/2/2010 in Maule, 1/4/2014 in Iquique and 16/9/2015 in Illapel

The manifestation of space climate in the geomagnetic field during the periods concerned is defined by the Kp magnetic activity index as shown in Figure 2 for the months previous to the three earthquakes: Maule 2010 (Dec 12, 2009 to Mar 15, 2010), Iquique 2014 (Jan 1, 2014 to Apr 15, 2014) and Illapel 2015 (Jul 1, 2015 to Sep 30, 2015). For Maule 2010 the magnetic activity reached a Kp index equal to or greater than 4 on only three isolated occasions, it is therefore considered a calm period; for Iquique 2014, activity was concentrated around Feb 19, 2014 while for Illapel 2015 the maximum activity was recorded between September 8 and 10. In all three cases, activity did not persist in time. In fact, according to figure 2, there is no evidence of an increase in the amount of external magnetic perturbations prior each earthquake.

3 Main magnetic evolution and frequency analysis

Magnetic measurements and analysis are carried out in this section. The main aim of this section is to use different magnetic methodologies and figure out which of them seems more earthquake-related. The stages correspond to the long-term magnetic evolution, the simple frequency analysis, wavelet and anomaly analysis. Stations used here are Putre (PUT), Easter Island (IPM, also known as Isla de Pascua), Los Cerrillos (CER), Pilar (PIL), Osorno (OSO) and Laboratorio antártico de radiación cósmica (LARC). See Figure 1 for their location and information of PUT, CER and LARC in Table 1. In the case of PUT and IPM, the Dobrovolsky area and the earthquake distances will be used in the following subsubsections (Table 2).

3.1 Long-term magnetic records

A high correlation between the vertical component of the earth's magnetic field and seismic activity at the Putre station was found (Cordaro et al., 2018). That is why we seek to specify this behavior in a shorter time window than the period studied previously (1975-2010). In addition, the B_z component in Easter Island (IPM) station is also used because it has not been thoroughly investigated (Note that the IPM station was closed in 1968 and subsequently reactivated in 2008 by the French INTERMAGNET Group and the Meteorological Service of Chile) (Chulliat et al., 2009, Soloviev et al., 2012). The Putre observatory is at 18°11'47.8S, 69°33'10.9W, 3,598 m.a.s.l. (meters above sea level); and it is located on the western edge of the South American Plate. This zone includes the South Atlantic Magnetic Anomaly (SAMA), the center of which is 1,700 kilometers east of this observatory. The measurements confirm low Bz values at the station Putre. The instrument error of the geomagnetic measurements is of the order of 5 nT (Cordaro et al 2012). IPM is located at 27.1°S, 109.2W, 82,83 m.a.s.l, on the western edge of the Nazca plate, characterized as a hotspot (e.g. Vezzoli and Acoocella, 2009). OSO is located in the coordinates 40°20'24" S, 74°46'64" W and PIL at 31°40'00.0" S, 63°53'00.0" W (Figure 1).

In the Putre, a diminution in the values of the whole magnetic field and each of its components is found. This can be attributed to the fact that Putre observatory is influenced by the South Atlantic Magnetic Anomaly, while on Easter Island the influence of SAMA is weaker (Storini et al., 1999). These magnetic influences are also found in Los Cerrillos observatory. The scientific and technical characteristics of the Putre (PUT) and Los Cerrillos observatories, i.e. location, altitude, atmospheric depth, type of detectors, geomagnetic cutoff rigidities and operating times, may be found in Refs. (Cordaro et al., 2012, Cordaro et

al., 2016) while for Easter Island (IPM) the information is available in SuperMag Network (Chulliat et al., 2009, Gjerloev, 2012). The main characteristics for the observatories i.e., location, altitude, atmospheric depth, type of detector, and operations time, are shown in Table 1.

Measurements of the B_z component are represented in Figure 3. We observe that similar gradients in Iquique 2014 and Illapel 2015 to those found in Maule 2010, giving rise to a jump in each case. It is known that these magnetic signals are generated by the earth's core and disseminated through the mantle, implying changes in its electrical conductivity (Stewart et al., 1995).

The jump in the B_z component for Maule 2010 was recorded in the Putre station on Jan 23, 2010 (purple solid line in Figure 3a), a time lapse of 36 days before the earthquake (solid red line) and the moment at which a change appears in the gradient or trend. It alters from a diminution of 225 nT in the period Oct 31, 2009 to Jan 23, 2010, to a less abrupt diminution of 30 nT between Jan 23, 2010 and Apr 3, 2010; prior to the jump on Jan 16, 2010 there is a small, abrupt diminution from -5048 nT to -4927 nT. Discounting this small, abrupt diminution, the delta between the gradients falls from -4960 nT to -4926 nT, delta = 34 nT as it is shown in Figure 3a.

For Iquique 2014 the jump recorded in Putre (Figure 3b) occurred on Dec 27, 2013 (purple solid line), a time lapse of 96 days before the earthquake (red solid line). A change appears in the gradient on this date from a diminution of 123 nT in the period Nov 14, 2013 to Dec 27, 2013, to a diminution of 113 nT between Dec 27, 2013 and Apr 15, 2014; the jump presents a change from -7355 nT to -7235 nT, delta = 120 nT as it shown in Figure 3. For Iquique 2014 the jump measured at IPM occurred on Dec 31, 2013, a time lapse of 91 days before the earthquake (Figure 3c). The trend shows a slight increase between Sep 30, 2013 and Jan 3, 2014, from -19116 nT to -19104 nT, while a further slight increase occurs in the period Jan 3, 2014 to May 6, 2014, from -19101 nT to -19099 nT. Note that the size of the jump was -3 nT as it is shown in Figure 4. For Illapel 2015 the jump measured at IPM occurred on Aug 31, 2015, a time lapse of 16 days before the earthquake. The trend shows a slight diminution between Aug 31, 2015 and Sep 20, 2015, from -19054 nT to -19072 nT, a jump of -11 nT, as one can observe in Figure 3d.

3.2 Simple Fourier analysis

Regarding the frequency analysis, the frequency spectrum values were analyzed for the Maule, Iquique and Illapel earthquakes using the second derivative of the vertical component at PUT and IPM stations. Fundamental frequencies before these earthquakes ranged from 5.606 to 3.481 μ Hertz or from 1 cycle / 48.9 hours to 1 cycle / 79.13 hours (Figure 4a). The increase in one or a group of frequencies reflects the oscillations of the radial magnetic field whose oscillation period takes from ~2 to ~4 days. Specifically, in the Maule event, peaks for the frequencies 4.747; 5.064 and 5.154 μ Hz were recorded (blue squares in Figure 4a). In Iquique peaks of 4.611; 4.882 and 5.154 μ Hz were recorded (black dots in Figure 4a), and for Illapel, 3.739; 4.630 and 5.520 μ Hz (red rhombuses in Figure 4a).

In order to identify a temporal domain where these frequencies arise, FFT is applied each 20 days as a first approximation (Figure4b, c). Before the Iquique 2014 event a jump in intensity was observed associated with the frequency of 5.154 μ Hz for the period Dec 27, 2013 to Jan 11, 2014, i.e. after the jump (Figure 3b, Figure 4b). Similar frequencies (3.739 μ Hz) rise during Sep 1, 2015 to Sep 8, 2015 before the Illapel 2015 event (Figure 4c). These findings imply a more detailed methodology in order to study the origin of these frequencies.

3.3 Wavelet analysis

We have used the wavelet transformation to analyze localized versions of power within a geomagnetic time series. In this way, it can break down a time series into the time-frequency space, determine the dominant modes of variability and how they vary over time (Torrence and Compo, 1998). Here, the goal is to look for the rare variations that could not be attributed to space weather in the daily average measurements. According to Cordaro et al. (2018), the magnetic field's vertical component showed variations related to the Maule 2010 earthquake. That is why values of the vertical component of the geomagnetic measurements at the OSO station were considered. Note that the OSO station is the closest station to the main earthquake. In order to avoid the space weather influence, the highest variations were not considered. One way to consider these two restrictions is by using statistical analysis. For example, a lower and upper threshold could be defined by using the standard deviation. Consider higher magnetic

peaks, but not too meaningful because they could be related to space weather conditions. An example of this statistical analysis when an upper threshold of 2 standard deviations is used can be found in Figure 5, in which panel (a), (b), and (c) stand for Maule 2010, Iquique 2014, and Illapel 2015 earthquakes, respectively. For Maule 2010, the spectral analysis shows a dramatic increase 30 days before Maule earthquake and a decrease ten days after the earthquake occurrence (yellow and green arrows in Figure 5a). The frequencies that rise comprise a range close to 3-5 μ Hz. Note that no other significant increase is seen during the two years of measurements between days -365 up to -30 and between 10 to 365 is clear that there is no significant rise of frequencies (blue shades in Figure 5a). Panel (b) of Figure 5 shows the results for Iquique 2014, which is characterized by two peaks. The first one rises 89 days before the earthquake (yellow arrow in Figure 5b), while the second one occurs after the Iquique earthquake (after the red line, which indicates the earthquake day). The Illapel case is also characterized by two peaks, as it is shown in panel (c) of Figure 5. The first rise occurs ~159 days before the earthquake (yellow arrow in Figure 5c), while the second rise is 52 days before the main earthquake (grey arrow in Figure 5c). Despite this promising methodology that considers the daily average and the upper threshold, an improved implementation of physical (i.e., space weather conditions) and statistical (adequate definition of anomalies and frequency considerations) analysis is required.

Finally, let us point out that more profoundly and sophisticated multiresolution wavelet analysis on time series related to earthquakes has been performed by Telesca et al. (Telesca et al. 2004 & Telesca et al. 2007). This kind of study will be considered in future works.

3.4 Anomaly analysis

In order to identify and discriminate external variations from those that could be considered as lithospheric (variations with lithospheric origin), this subsection handles the definitions of anomalous variations. This definition will be obtained considering the external perturbation by using the Dst index (http://wdc.kugi.kyoto-u.ac.jp). Then, spectral analysis will be performed. Additionally, the data used in this subsection is standard and comes from the supermag network (http://supermag.jhuapl.edu/). The data has a sampling frequency of one data per minute, and a period of one year before and one year after each earthquake was chosen.

3.4.1 Magnetic threshold definition

In the method of cumulative magnetic anomaly on the surface of earth, we used statistically an atypical or anomalous value, that is, data that is quite far from the average values of the sample. So, we compare real values of B_i with a more representative value of the sample, its average $\underline{B_i}$. We will call the difference between the two as the magnetic residual ΔB_i. By using the distribution of data, we can define when a value is atypical or anomalous in a normal distribution by statistical definitions of quartiles and outliers.

On the one hand, we create a filter that eliminates the frequencies averaged near Nyquist and establishes a filter that eliminates high frequencies (stochastic filter). The option was to consider a weighted moving average of five points: $\bar{B}_i = aB_{i-2} + bB_{i-1} + cB_i + bB_{i+1} + aB_{i+2}$. Here, other researchers have used cubic splines instead of moving average (e.g. De Santis et al., 2017). In our case we use $a = 0.07, b = 0.25$ and $c = 0.5 - 2a$. The uncertainty of the Flux-gate magnetometers (supermag) from OSO and PIL station is $\delta B_i = \pm 0.1\ nT$, while the error of the moving average implementation is $\delta \bar{B}_i = \pm 0.1\ nT$. As residual values are defined as the difference between real and smoothed data ($\Delta B_i = B_i - \bar{B}_i$), the total error propagation of residual is $\delta B_i + \delta \bar{B}_i = \pm 0.2\ nT$.

Let us comment that the error of propagation is used to define a threshold that determines when a residual is considered anomalous or not. For instance, in statistics 0.6745σ represents 50% of the data that is closer to the average (where σ is the standard deviation). This means that residuals less than $0.6745\sigma\ nT$ are closer to the average and therefore are more common. As residuals are considered anomalous when they are unlikely, anomalous data should be defined as those residuals larger than $0.6745\sigma\ nT$. By adding the error propagation as condition ($0.6745\sigma + 0.2\ nT$), and considering that the standard deviation is similar to $\sigma \sim 0.1\ nT$, the percentage of residuals that meets this condition are considerably smaller than the 50% of the data (less common). Thus, residuals ΔB_i are consider anomalous (ΔB_{ai}) when

$$|\Delta B_i| \geq 0.6745\sigma + 0.2\ nT \quad (1).$$

The vertical magnetic thresholds found are 0.2246995 nT at OSO (Feb 27, 2009 - Feb 27, 2011), 0.2362868 nT at PIL (Apr 01, 2013 – Apr 01, 2015) and 0.2352825 nT at PIL (Sep 16, 2014 – Sep 16, 2016). These threshold are ~ 6, ~4.5 and ~4.5 times larger than each σ respectively. This means that each anomaly above this threshold meets the 3σ criteria (a valid observation). Furthermore, the thresholds are close to the 5 σ criterion which corresponds to the standard discovery criteria in the physical sciences, for example this criterion was used in the discovery of the Higgs boson (https://home.cern/news/news/physics/higgs-within-reach)

Regarding the external contribution, the data considered are for quiet periods Dst <10 nT, and only quiet magnetic data between 16:00 to 05:00 local time (Hitchmn et al., 1998). Some researchers who have used satellites consider only the time periods in which the DST index is less than or equal to 20 nT (e.g. Marchetti and Akhoondzadeh, 2018), or equal to 10 nT (e.g. De Santis et al., 2017). That means that the space weather conditions could invalidate the anomaly condition defined in equation (1) if DST > 10 nT. Then, the proper application of equation (1) is linked to those times where space weather activity is low. That is when Dst < 10 nT and quiet magnetic data (16:00 to 05:00 local time).

Finally, the fourth filter process considered corresponds to the study of the recurrence of anomalous residuals. For instance, if the anomalous threshold is three times the standard deviation, it implies that one of every 740 data is anomalous. It is the same as two every 1480. As this work uses 1440 data per day, it is expected that ~ two will be anomalous per day. In terms of probabilities, it is the same to $P_{day} \approx 0.0014$. Contrariety, if one single day shows, let's say, 30 anomalies, the probability is $P_{30} = \left(P_{day}\right)^{30} \sim 10^{-86}$. This means that the occurrence of 30 anomalies is virtually zero, and it could imply that the previous filters (anomaly definition, DST, and quiet time) failed during that day. Then, it is not possible to consider those days where the number of anomalies per day is considerably larger than 2. That is why days with larger than ten anomalies are not considered valid.

3.4.2 Spectrogram

The filtered data correspond to a strong candidacy of lithospheric magnetic origin. This means that any spectral analysis could reveal lithospheric variations. That is why simple spectrograms analysis is performed. The spectrogram corresponds to the application of the moving Fourier transform. Here, the temporal window size is 1 month with a 50% of overlap, which holds a reasonable spectral and time resolution (see Rabiner and Schafer (1980) and Oppenheim et al. (1999) for spectrogram theory and application). The OSO and PIL spectrograms for Maule 2010, Iquique 2014 and Illapel are shown in Figure 6.

In the Maule 2010 event, the spectrogram of the vertical magnetic component at the OSO station is shown in Figure 6a. There is no significant rise of frequencies during the period before the Maule event (before ~ January 10, 2010). Nevertheless, a dramatic increase during the period January 10, 2010 - May 02, 2010, occurs. Specifically, the rise of frequencies lies in the range ~1 - 2.2 mHz. The onset of this rise (January 10) occurs more than one month before the Maule earthquake (February 27) and lasts almost four months. That means that the spectral density reduces their activity after ~2 months of the earthquake.

The spectrogram for Iquique 2014 is characterized by two peaks (Figure 6b). The first one corresponds to September 22, 2013, and the second one in ~ March 08, 2014. Here, the frequency range comprises between ~ 1.2 to 2.7 mHz, which is similar to that found in the Maule spectrogram. However, the main peak occurred during March, which is characterized by a dominant frequency close to 2.5 mHz, while the dominant frequencies in Maule 2010 are close to 1.2 and 2.2 mHz, respectively. There is an additional difference compared to the Maule event: The rise of frequencies in Iquique 2014 comprises a significant decrease (or "valley") in the spectral density, which last almost two months (~ November 09, 2013-Dec 27, 2013). It means that the second rise of frequencies lasts more than four months (~ December 27, 2013-May 03, 2014), which is a similar duration compared to the frequency rise of Maule 2010.

The final spectrogram is found in Figure 6c, which corresponds to the Illapel 2015 event. Here, it can be seen that almost the entire period was characterized by close to zero frequency variations. Nevertheless, the frequency rise is similar to that obtained in Maule 2010. That is, significant frequencies

rise only on dates close to the earthquake event. The rise lasts almost three months (~ August 06, 2015 - October 27, 2015). It is important to note that the gap between September 2015 is due to the strong spatial weather activity. Despite this, it is clear that the earthquake occurrence lies during periods of high-frequency activity, which is a similar feature compared to Maule 2010 and Iquique 2014.

Panels (a)-(c) of Figures 6 show that three strong earthquakes (Maule 2010, Iquique 2015, and Illapel 2015, respectively) occurred during the rise of ultra-low frequencies of the vertical magnetic component. It is important to highlight that these frequencies (mainly 1-2.5 mHz) vanish or reduce their intensity values during other time periods. This is in agreement with other authors who have claimed that ultra-low frequencies accompanied and the increases of the number of magnetic anomalies are related to the earthquake preparation process (e.g., De Santis et al., 2017). It means that anomalous peaks produce the magnetic oscillations in the magnetic records. By following the Venegas-Aravena et al. (2010) findings, the number of these peaks also should increase (decrease) in time before (after) earthquake occurrences.

3.4.3 Cumulative daily anomalies

By following the anomaly definition (subsection 3.4.1), it is possible to find out the daily number of anomalies- For example, in Figure 7 is shown the case of OSO station. Black dots follow a stable linear increase in the number of cumulative anomalies (red line). Nevertheless, this tendency breaks close to Jan 11-12, 2010. From that day up to the first week of April, the numbers of anomalies experience a dramatic increase. In the middle of this increase, the Maule earthquake hit (Feb 27, 2010). By subtracting the initial linear tendency and comparing it to PIL station (Iquique 2014 and Illapel 2015), the sigmoidal feature is clearer (Figure 8). The anomalies start to increase prior to each earthquake. For example, this increase started ~47 days before the Maule 2010 earthquake, ~90 days before the Iquique 2014 earthquake and ~60 days before the Illapel 2015 earthquake (Figure 8).

Other researchers have used very different implementations, definitions, methodologies, and data in order to find out these anomalies. For example, Marchetti and Akhoondzadeh, (2018) have also found a sigmoidal signature in the anomalies of the Y components recorded by different satellites for the Mexico 2017 earthquake. In order to compare Mexico 2017 with Maule 2010, Iquique 2014 and Illapel 2015, the initial linear trend has been removed (Figure 9). The initial onset of anomalies increased close to 60 day prior to the Mexico 2017 earthquake. Note that in the four cases, the sigmoidal features are almost the same: a linear stable number of anomalies characterize the initial period. Then, a dramatic increase in the number of daily anomalies is followed by the main earthquake. This time is different in each earthquake but it lies between 50 – 90 days after the initial anomalies increase. After the seismic events happen, the cumulative numbers behave not similarly. For example, in the Mexico 2017 earthquake, the anomalies remain stable, while in the Maule 2010 still is increasing in a less dramatic manner. At the end of the OSO measurements, several anomalies appear, but it is not clear that these events could be related to other seismic events. In order to understand the physics that lies in these events, a theoretical mechanism is required.

4.-Magnetic anomalies and fracture mechanics by considering the seismo-electromagnetic theory.

The frequency analysis (Figure 5, 6) and cumulative number of magnetic anomalies (Figures 7, 8, 9) shows an increase (spectral intensity and anomalies number) before each earthquake occurs. In the anomalies case, a clear sigmoidal feature rises in Maule, Iquique and Illapel, which is a similar behavior recorded in the Mexico earthquake (Figure 9, Marchetti and Akhoondzadeh, (2018)). This indicates that anomalies behavior could correspond to a lithospheric origin. Currently, it has been shown that the origin of these anomalies is associated with the cracking (or micro-cracking) of the semi-fragile-ductile part of the lithosphere (crust) due to changes in stress (Venegas-Aravena et al., 2019). Typically, strain appears when solids undergo loads or stress accumulation. However, micro-cracks rise specifically when solids do not hold more deformation and prior to the main failure (e.g., Stavrakas et al., 2019, Li et al. 2020). Experimentally, it has been shown that these conditions break the electrical neutrality within materials and generate an electrical flux through rocks in a process known as pressure stimulated currents or PSC (e.g., Anastasiadis et al., 2004). Furthermore, it has been shown that PSCs can explain that the fractal nature of cracks is sufficient to generate the frequency spectrum, co-seismic variations, the generation and behavior of anomalies, and variation in the ionosphere in a theory known as seismo-electromagnetic theory (Venegas-Aravena et al., 2019). Regarding the time evolution of magnetic anomalies, De Santis et al.

(2011) have shown that the sigmoidal shape is due to a manifestation of the stress changes when it is reaching a critical point. Nowadays, theoretical development, geodynamical measurements, and experimental studies have shown that the sigmoidal shape appears as a consequence of the dramatic increase in the number of micro cracks (at a depth of few tens of kilometers) prior the main earthquake ruptures (De Santis et al., 2015, Stavrakas et al., 2019, Venegas-Aravena, et al., 2019).

A schematic representation of the crack generation in the geodynamical context can be seen in figure 10. At the initial time $t = t_0$ the intact lithosphere undergoes a uniaxial non-constant stress σ (Figure 10a). Then the first signs of micro cracks appear at $t = t_1$ due the increase of the stress (Figure 10b). When the lithosphere can not hold more deformation, a dramatic increase in the crack generation appear throughout the lithosphere ($t = t_2$ in Figure 10c). At this point ($t = t_3$ in Figure 10d), the crack generation is not sufficient to release the excess of uniaxial stress. Then the lithosphere cannot release energy by neither deformation nor crack generation mechanism. That is why the rupture (earthquake) occurs (green area in Figure 10d) at $t = t_4$. After the main rupture, another aftershock occurs (green smaller patches within the fault in Figure 10e). Nevertheless, the number of anomalies start to decrease. Finally, the micro crack generation stops because the deformation is sufficient to handle the lithospheric response to non-constant uniaxial stress (Figure 10f).

Additionally, Venegas-Aravena et al. (2019) found that the increase in the number of anomalies are controlled by the same fractal nature that drives the micro crack generation. This means that the frequency of the electrical flux could cover several magnitude orders. For example, figures 4, 5, and 6 are characterized for the rise of different frequencies (micro to mili-hertz), which are known as ultra-low-frequency (ULF), prior main earthquakes. These frequencies ranges were also found and described by others researches as Fenoglio et al. (1995), Vallianatos and Tzanis (2003), Fraser-Smith (2008), De Santis et al. (2017), Cordaro et al. (2018), among others.

Finally, it has been concluded that there must be precursory magnetic anomalies of the order of 0.1 nT related to earthquakes on the earth's surface (e.g. De Santis et al, 2017, Chernogor, 2019, Venegas-Aravena et al., 2019). In the previous section, it was found that the minimum value to define an anomaly was close to 0.2 nT. Therefore, this experimental result is in agreement with the theoretical value obtained. Consequently, as the seismo-electromagnetic theory indicates, those magnetic anomalies may have a lithospheric origin. Furthermore, the behavior of all these anomalies has a preceding increase similar to that of other seismic events that use different data and methods (e.g., De Santis et al., 2019; De Santis et al., 2019b and references therein).

5.- Discussions and Conclusions

The most significant characteristics of the magnetic field and its variations are found in the z-component, which we have observed and recorded at the Putre and IPM observatories. The previous measurements show that there is evidence of a progressive increase in the phenomenon known as the South Atlantic Magnetic Anomaly (SAMA) (Cordaro et al., 2019). As expected, it generates a significant deviation in the intensities present in the OP station as it is shown in the magnetic iso-values (Figure 1). Combining this information with data from the IPM station, the behavior of the radial component of the geomagnetic field for the three most significant seismic events in the Chilean Pacific sector during the period 2010-2015 was recorded, and it corroborates the magnetic relation with seismology shown in Potirakis et al. (2016), Contoyiannis et al. (2016), De Santis et al. (2017), which have been used other methods.

The normal magnetic trend showed some long-term variations. For example, there were breaks in the trend or jump of B_z, followed by a time-lapse, and seismic movement as one can observe Figure 3. These jumps occur in different forms: in Putre they are significant, reaching values of tens of nT, while in IPM the jump is barely 10nT. The time lapse between each jump and the seismic event differs in each event. For Maule 2010 it was 36 days, for Iquique 2014 it was 96 days, and for Illapel 16 days. This time difference may be due to an important factor: it appears that the jump is not equally strong in the three events, since the jump before the Iquique 2014 event was considerably. weaker than the one before Illapel 2015, and preceded the event by a longer time lapse (96 days). The more abrupt jump recorded in Illapel was followed by a shorter time lapse (16 days). These changes are notorious, that is why a first approach by using frequency analysis was done.

Specifically, significant frequencies data obtained for Maule earthquake Chile, 2010, range from 4.747 to 5.154 μ Hz, for Tohoku earthquake. Japan 2011 from 4.747 to 5.606 μ Hz, for Sumatra earthquake

Indonesia 2004 from 3.481 to 5.425 μ Hz (Cordaro, et al 2018). These fundamental frequencies were detected before the earthquake in the areas of Pacific Ocean in the Southern Hemisphere, in the Eurasian (2011) and Philippine (2004) areas in the Northern Hemisphere. Now these significant frequencies are obtained again in different places and time on earth: in Iquique 2014, peaks of 4.611, 4.882, and 5.154 μ Hz and for Illapel 2015, 3.739, 4.630, and 5.520 μ Hz (Figure 4). Up to this point, the rise of these frequencies could be thought as a normal magnetic behavior with a high degree of coincidence. That is why, other methodologies were performed in order to clarify the origin of these frequencies.

From now on, in order to avoid bias or technical malfunction, we decided to use different stations that belong to an international network with open source data (supermag). These stations (OSO and PIL) were the closest to the three earthquakes that had continuous measurements. The time period was 1 year before each earthquake and 1 year after, giving 6 years of combined measurements where the frequency sample was 1 data per minute.

The first approach was performed by using wavelet analysis at OSO station. Here, in order to avoid normal variations and external perturbation, daily average values were performed by imposing a lower and upper restriction before applying wavelet analysis. The Figure 5a shows the increase of the frequency range (> 2 μ Hz) ~30 days before the Maule 2010 earthquake. These frequency activities last up to ~10 days after the earthquake. Similar frequency results were obtained for Iquique 2014 (Figure 5b) and Illapel 2015 (Figure 5c). Despite the abovementioned results, the previous restrictions might be seen as arbitrary. That is why we moved to a stricter, stronger and bias-free methodology. Besides, three facts should be taken into account. The first one is considering the physics-based filter processes, which remove most of the noise and external disturbances. Thus, it allows performing more simple frequency analysis as the moving Fourier transform (spectrogram). The second one is the tridimensional representation. This is important because it is possible to observe the relative frequency intensity differences in a proper way. Furthermore, the third one is that this spectrogram, and its tridimensional representation, allow us to compare our results to previous works in the field (for example, Cordaro et al., 2018).

The definition of magnetic anomalies was performed in subsection 3.4.1. There, the anomalous magnetic variations were defined by using statistical analysis. That is, one variation or peaks will be considered anomalous if it reaches values beyond a certain threshold, threshold defined by the same data. In order to avoid the external perturbations, Dst index and quiet time were considered. This gives six years of combined data with variations that could be associated to lithosphere or internal. An increase in the frequency range (~1 mHz) before each earthquake was obtained after applying spectrogram analysis (Figure 6). If we look at those periods not close to the earthquake's occurrences, almost no frequency activity was recorded. In addition, these frequencies cannot be considered as part of tidal effects because the last one belongs to a different frequency range (~0.01-0.06 mHz) (Casotto and Biscani, 2004, Park et al., 2005). Prior studies have shown that the frequencies in the range of ~mHz are also related to the earthquake preparation stage (Zlotnicki et al., 2001). This implies that Maule 2010, Iquique 2014, and Illapel 2015 occurred during very high-frequency activity comparable to those found by Zlotnicki et al. (2001). As the considered data is free of external perturbations, and earthquakes occurrences are within these frequencies' activations, the idea of the existence of lithospheric frequencies related to earthquakes are reinforced.

In order to compare these data with other results, we performed the count of the daily anomalies. Here, the anomalies behave as a sigmoidal function (Figure 7, 8, 9). In all of the earthquakes there was found a dramatic increase in the number of anomalies between 50 to 90 days before each earthquake. This long-term behavior is similar to those found in Nepal 2015 (De Santis et al., 2017), Mexico 2017 (Marchetti and Akhoondzadeh, 2018), Central Italy (Marchetti et al., 2019a), Indonesia 2018 (Marchetti et al., 2019b) or other big earthquakes worldwide (De Santis et al., 2019b). Note that the above-mentioned studies used satellite data in contrast with this study which employs ground-based magnetometers and different methodology. Additionally, the station selection followed the preparatory phase described by Dobrovolsky et al. (1979). This means that any magnetic station, close to impending earthquake (~ 1000 km), should detect anomalies or the lithospheric microcracking beneath Earth's surface. The horizontal distance of the preparation phase also agrees to geodetic findings. For example, Bedford et al. (2020) found a preparation phase characterized by a high increase in the strain close to ~1000 km in subduction margin. Note that the dates when anomalies rise dramatically are Feb 6, 2010 for Maule and Jan 8, 2014 for Iquique as it is shown in Figure 8. These dates match well compared to the onset of critical seismicity throughout the concept of characteristic precursory minima (β) in the framework of the Natural Time Analysis. For instance, Feb 1, 2010 and Dec 28, 2013 respectively (Sarlis et al., 2015). In addition, Figure 6b shows that the second (main) rise of frequencies begins on Dec 27, 2013. On the other hand, it is possible to observe that the onset of a

second rise in the cumulative number of anomalies for the Mexico 2017 earthquake is close to the day 118 (Figure 9) that corresponds to Jul 28, 2017. Our date is almost the same date (27 July, 2017) obtained by Sarlis et al. (2019) by applying the critical seismicity methods. It is then possible to claim that these similarities among frequencies, cumulative anomalies, and seismicity features should be considered different manifestations of a lithospheric phase transition.

By considering the above and the four filters applied (DST, quiet daily time, stochastic and recurrences) which led the definition of residual anomalies, it is possible to explain our results in terms of the physical mechanism described in the seismo-electromagnetic theory. This scheme explains different empirical observations that indicate a direct relation between magnetic fields and earthquakes in which one the essential group of measurement corresponds to the recording of ultra–low-frequency magnetic signal, mainly close to millihertz and microhertz (Venegas-Aravena et al., 2019, 2020). It is important to note that this theory considers the microcracking process (due to stress changes in the semi-brittle–ductile regime) as a fundamental physical unit because it has been widely studied their electrical properties (e.g., Triantis et al., 2020) or their influence in the propagation of the main failure (e.g., McBeck et al., 2021). Under this concept, the anomalies correspond to the manifestation of the crack or micro crack within the lithosphere which allows the flux of electrical current. Due to the Zener-Stroh mechanism (e.g., Stroh, 1955, Ma et al., 2011), while changes in the seismicity rate are due to changes in the b-value (Venegas-Aravena et al., 2020) which could generate seismic foreshock or slow slips as in Iquique 2014 (e.g., Herman et al., 2016). Also, this theory considers the main earthquake as a crack that releases seismic energy as coseismic magnetic signals (Kanamori, 1977, Utada et al., 2011). The temporal evolution of these cracks and its relation to the sigmoidal magnetic anomalies' behavior can be seen in Figure 10. The framework of this theory states that the micro cracks appear as a consequence of the excess of shear stress that cannot be released by the lithospheric deformation (Venegas-Aravena et al., 2019). Then, frequencies rise and anomalies behavior should be considered as a manifestation of the internal lithospheric collapse at the last stage (preparation stage) of the seismic cycle, when solids cannot hold more strain. Since the electrical currents are intense after the linear regime (Triantis et al., 2020), the phase transition described by Sarlis et al. (2019) could be considered a (physical and statistical) manifestation of the changes in the semi-brittle-ductile regime. Then, they can generate the above-mentioned magnetic anomalies found in this work.

Regarding the mechanism that generates the micro-cracks, we found that the minimum value to define an anomaly was close to 0.2 nT, and this experimental result is in agreement with the theoretical value obtained in Venegas-Aravena et al. (2019), where a ~0.2 nT rise when cracks are created at the semi-brittle ductile regime (depth of 10-20 km) (Scholz, 2001, Sun, 2011).

Let us mention that the frequencies obtained by the Fourier analysis and anomalies are inherent to the lithosphere. The variation of the low frequencies before the earthquake in the magnetic field is part of the ionosphere-atmosphere-lithosphere coupling. Previously, we have shown that the frequencies in μHz are related to the Maule earthquake in 2010 (Mw 8.8) (Cordaro et al. 2018). According to Vallianatos and Tzanis (2003), the magnetic field frequencies, which are possibly related to earthquakes, could span a range of at least three orders of magnitude. Specifically, they have detected a range of frequencies between 5 - 100 *mHz* before one month before earthquakes based on the Ionosphere-Lithosphere-atmosphere coupling.

We also remark that the possibility to predict the future occurrence of these seismic events is not yet possible because the seismological mechanism of seismic movements is not yet precise. This means that the role played by the fault's rupture parameters are not well understood. Specifically, the heterogeneities, frictional properties, asperities and fault roughness are relevant to increase the complexity of the nucleation process that determine the released energy, earthquake size, fracture energy and ground motion (e.g., Saltiel et al., 2017, Selvadurai, 2019, Heimisson, 2020). However, a correlation does appear to exist between a cumulative number of magnetic anomalies, time-lapse, frequency arise, and the Maule 2010, Iquique 2014, and Illapel 2015 earthquakes. This methodology could be used as a tool to show the behavior of some geophysical variables to indicate plate movements in the future. This condition, based on the increase of low frequencies in the range of $(\mu Hz - mHz)$ suggests that these magnetic variations in the radial component are probably a necessary but not sufficient condition on the Chilean margin. Further investigations on this subject are required.

The next experimental step in this analysis is to gather the measuring instruments of the network (magnetometers, Neutrons, others) and their variables recorded in the lithosphere, ionosphere, magnetosphere, cosmic rays particles,) as neutrons, making a synapse or communication between them, in real time (Machine Method Learn and others), in order to detect, directions, intensities, start and end of

frequencies, magnetic clusters, anomalies, or others, that could allow us to generate a warning prior to a seismic movement.

Acknowledgments

The authors thank Dr. L.A. Raggi (INCAS – Universidad de Chile) for their collaboration and support. The fluxgate magnetometer at Putre-Incas Observatories is partially supported by Universidad de Chile and Universidad de Tarapacá. The LARC observatory receives support from the Chile/Italy collaboration via Universidad de Chile and PNRA (Italy). We also thank INACH for partial support. The results presented in this paper rely on data collected at magnetic observatories. We thank the national institutes that support them and INTERMAGNET for promoting high standards of magnetic observatory practice (www.intermagnet.org). D. Laroze acknowledges partial financial support from Centers of Excellence with BASAL/ANID financing, Grant AFB180001, CEDENNA. E. G. Cordaro acknowledges Marcela Larenas and Francesca, Beatriz and Enrique for outstanding support to carry out this work.

References

Abad, M., Izquierdo, T., Cáceres, M., Bernárdez, E., Rodriguez-Vidal, J.: Coastal boulder deposit as evidence of an ocean-wide prehistoric tsunami originated on the Atacama Desert coast (northern Chile). Sedimentology 67, 1505–1528, doi: 10.1111/sed.12570, 2020.

Anastasiadis, C., Triantis, D., Stavrakas, I., and Vallianatos, F.: Pressure Stimulated Currents (PSC) in marble samples. Ann. Geophys., 47, 21–28, doi: 10.4401/ag-3255, 2004.

Balasis, G. and Mandea, M.: Can electromagnetic disturbances related to the recent great earthquakes be detected by satellite magnetometers? Tectonophysics, 431, 173–195, doi: 10.1016/j.tecto.2006.05.038, 2007.

Bedford, J.R., Moreno, M., Deng, Z., Oncken, O., Schurr, B., John, T., Báez, J.C. and Bevis, M.: Months-long thousand-kilometre-scale wobbling before great subduction earthquakes. Nature 580, 628–635 (2020), doi: 10.1038/s41586-020-2212-1, 2020.

Blagoveshchensky, D. V., Maltseva, O. A., and Sergeeva, M. A.: Impact of magnetic storms on the global TEC distribution, Ann. Geophys., 36, 1057–1071, doi:10.5194/angeo-36-1057-2018, 2018.

Bloxham, J., Zatman, S. and Dumberry, M.: The origin of geomagnetic jerks. Nature 420, 65-68 (7 November 2002). doi: 10.1038/nature01134, 2002.

Cartwright-Taylor, A., Vallianatos, F., and Sammonds, P.: Superstatistical view of stress-induced electric current fluctuations in rocks, Physica A, 414, 368–377, 2014.

Carvajal, M., Cisternas, M. and Catalán, P.A.: Source of the 1730 Chilean earthquake from historical records: Implications for the future tsunami hazard on the coast of Metropolitan Chile, J. Geophys. Res. Solid Earth, 122, 3648–3660, doi:10.1002/2017JB014063, 2017.

Casotto, S. and Biscani, F.: A fully analytical approach to the harmonic development of the tide-generating potential accounting for precession, nutation, and perturbations due to figure and planetary terms. AAS Division on Dynamical Astronomy, April 2004, vol. 36(2), 67, 2004.

Chernogor, L.F.: Possible Generation of Quasi-Periodic Magnetic Precursors of Earthquakes. Geomagn. Aeron. 59, 374–382 (2019), doi: 10.1134/S001679321903006X, 2019.

Christopoulos, S.-R. G., Skordas, E. S, and Sarlis, N. V.: On the Statistical Significance of the Variability Minima of the Order Parameter of Seismicity by Means of Event Coincidence Analysis, Applied Sciences 10, 662 (2020), doi: 10.3390/app10020662, 2020.

Chulliat, A., Lalanne, X., Gaya-Pique, L.R., Truong, F. and Savary, J.: The new Easter Island magnetic observatory. Proceedings of the XIIIth IAGA Workshop on Geomagnetic Observatory Instruments, Data Acquisition and Processing, edited by J. J. Love, 271 pp., U.S. Geological Survey Open-File Report 2009-1226, 2009.

Contoyiannis, Y., Potirakis, S.M., Eftaxias, K., Hayakawa, M., Schekotov, A.: Intermittent criticality revealed in ULF magnetic fields prior to the 11 March 2011 Tohoku earthquake (Mw = 9). Physica A 452, 19–28, doi: 10.1016/j.physa.2016.01.065, 2016.

Cordaro, E.G., Olivares, E., Gálvez, D., Salazar-Aravena, D., Laroze, D.: New 3He neutron monitor for Chilean osmic-ray observatories from the Altiplanic Zone to the Antarctic zone. Adv. Space Res. 49, 1670, doi: 10.1016/j.asr.2012.03.015, 2012.

Cordaro, E.G., Gálvez, D. and Laroze, D.: Observation of intensity of cosmic rays and daily magnetic shifts near meridian 70° in the South America. Journal of Atmospheric and Solar-Terrestrial Physics. Volume 142, May 2016, Pages 72–82. doi: 10.1016/j.jastp.2016.02.015, 2016.

Cordaro, E.G., Venegas, P. and Laroze, D.: Latitudinal variation Rate of Geomagnetic Cutoff Rigidity in the active Chilean convergent margin. Annales Geophysicae Angeo-2017-176. 2018, doi: 10.5194/angeo-36-275-2018, 2018.

Cordaro, E.G., Venegas-Aravena, P. and Laroze, D.: Variation of geomagnetic cutoff rigidity in the southern hemisphere close to 70°W (South-Atlantic Anomaly and Antarctic zones) in the period 1975-2010, Advances in Space Research, https://doi.org/10.1016/j.asr 2018.12.019, 2019.

De Santis, A., De Franceschi, G., Spogli, L., Perrone, L., Alfonsi, L., Qamili, E., Cianchini, G., Di Giovambattista, R., Salvi, S., Filippi, E., Pavón-Carrasco, F.J., Monna, S., Piscini, A., Battiston, R., Vitale, V., Picozza, P.G., Conti, L., Parrot, M., Pinçon, J.-L., Balasis, G., Tavani, M., Argan, A., Piano, G., Rainone, M.L., Liu, W. and Tao, D.: Geospace perturbations induced by the Earth: The state of the art and future trends. Physics and Chemistry of the Earth, Parts A/B/C, Vol. 85–86, Pages 17-33, doi: 10.1016/j.pce.2015.05.004, 2015.

De Santis, A., Balasis, G., Pavón-Carrasco, F.J. Cianchini G. and Mandea M.: Potential earthquake precursory pattern from space: The 2015 Nepal event as seen by magnetic Swarm satellites. Earth and Planetary Science Letters 461 (2017) 119–126. Doi: 10.1016/j.epsl.2016.12.037, 2017.

De Santis, A., Marchetti, D., Pavón-Carrasco, F.J., Cianchini, G., Perrone, L., Abbattista, C., Alfonsi, L., Amoruso, L., Campuzano. S.A., Carbone, M., Cesaroni, C., De Franceschi, G., De Santis, A., Di Giovambattista, R., Ippolito, A., Piscini, A., Sabbagh, D., Soldani, M., Santoro, F., Spogli, L. and Haagmans, R.: Precursory worldwide signatures of earthquake occurrences on Swarm satellite data. Sci Rep 9, 20287 (2019), doi: 10.1038/s41598-019-56599-1, 2019.

De Santis, A., Marchetti, D., Spogli, L., Cianchini, G., Pavón-Carrasco, F.J., De Franceschi, G., Di Giovambattista, R.,Perrone, L., Qamili, E., Cesaroni, C., De Santis, A., Ippolito, A., Piscini, A., Campuzano, S.A., Sabbagh, D., Amoruso, L., Carbone, M., Santoro, F., Abbattista, C. and Drimaco, D.: Magnetic Field and Electron Density Data Analysis from Swarm Satellites Searching for Ionospheric Effects by Great Earthquakes: 12 Case Studies from 2014 to 2016. Atmosphere2019 ,10, 371; doi: 10.3390/atmos10070371, 2019b.

Diego, P., Storini, M., Parisi, M. and Cordaro, E.: AE index variability during corotating fast solar wind streams. J. Geophys. Res.110, doi:10.1029/2004JA010715, 2005.

Dieminger, W., Hartmann, G.K. and Leitinger, R.: Geomagnetic Activity Indices. In: Dieminger W., Hartmann G.K., Leitinger R. (eds) The Upper Atmosphere. Springer, Berlin, Heidelberg, doi:10.1007/978-3-642-78717-1_26, 1996.

Dobrovolsky, I.R., Zubkov, S.I. and Myachkin, V.I.: Estimation of the size of earthquake preparation zones. Pure Appl. Geophys. 117, 1025–1044, doi: 10.1007/BF00876083, 1979.

Fenoglio, M. A., Johnston, M. J. S., and Byedee, J.: Magnetic and electric fields associated with changes in high pore pressure in fault zones: application to the Loma Prieta ULF emissions, J. Geophys. Res., 100, 12951–12958, doi: 10.1029/95JB00076, 1995.

Finlay, C.: Magnetohydrodynamics Waves, Encyclopedia of Geomagnetism and Paleomagnetism, Edited by D. Gubbins and E. Herrero-Berbera. Springer, Netherlands, 2007.

Florios, K., Contopoulos, I., Christofilakis, V., Tatsis, G., Chronopoulos, S., Repapis, C. and Tritakis, V.: Pre-seismic Electromagnetic Perturbations in Two Earthquakes in Northern Greece. Pure Appl. Geophys. 177, 787–799 (2020), doi:10.1007/s00024-019-02362-6, 2020.

Foppiano, A.J., Ovalle, E. M., Bataille, K. and M. Stepanova: Ionospheric evidence of the May 1960 earthquake over Concepción? Geofísica Internacional 47 (3), 179-183, 2008.

Fraser Smith, A.C.: Ultralow-frequency magnetic fields preceding large earthquakes, Eos Trans., 2008, vol. 89, no. 23, p. 211, doi: 10.1029/2008EO230007, 2008.

Freund, F.: Toward a unified solid-state theory for pre-earthquake signals, Acta Geophys., 58, 719–766, doi: 10.2478/s11600-009-0066-x, 2010.

Geller, R.J.: Earthquake prediction: a critical review. Geophysical Journal International, Volume 131, Issue 3, December 1997, Pages 425–450, doi: 10.1111/j.1365-246X.1997.tb06588.x, 1997.

Gjerloev, J. W.: The SuperMAG data processing technique, *J. Geophys. Res.*, 117 A09213, doi: 10.1029/2012JA017683, 2012.

Gubbins, D., Jones, A.L. and Finlay, C.C.: Fall in Earth's magnetic field is erratic. Science 312: 900–902 (2006), doi: 10.1126/science.1124855, 2006.

Han, P., Zhuang J., Hattori K., Chen C.-H., Febriani F., Chen H., Yoshino C., Yoshida, S.: "Assessing the Potential Earthquake Precursory Information in ULF Magnetic Data Recorded in Kanto, Japan during 2000–2010: Distance and Magnitude Dependences. Entropy 22, 859 (2020) doi: 10.3390/e22080859, 2020.

Hayakawa, M. and Molchanov, O.A. (eds.): Seismo Electromagnetics: Lithosphere-Atmosphere-Ionosphere Coupling. TERRAPUB, Tokyo, 2002.

Hayakawa, M., Schekotov, A., Potirakis, S., Eftaxias, K.: Criticality features in ULF magnetic fields prior to the 2011 Tohoku earthquake. Proc. Jpn. Acad. Ser. B, Phys. Biol. Sci. 91, 25–30, doi: 10.2183/pjab.91.25, 2015.

Heimisson, E.R.: Crack to pulse transition and magnitude statistics during earthquake cycles on a self-similar rough fault, Earth and Planetary Science Letters, Vol. 537, 1 May 2020, 116202, doi: 10.1016/j.epsl.2020.116202, 2020.

Heirtzler, J.: The future of the South Atlantic Anomaly and implications for radiation damage in space. Journal of Atmospheric and Solar Terrestrial Physics 64: 1701–1708, doi: 10.1016/S1364-6826(02)00120-7, 2002.

Herbst, K., Kopp, A., Heber, B.: Influence of the terrestrial magnetic field geometry on the Cutoff Rigidity of cosmic ray particles. Ann. Geophys. 31, 1637–1643, doi: 10.5194/angeo-31-1637-2013, 2013.

Herman, M.W., Furlong, K.P., Hayes, G.P. and Benz, H.M.: Foreshock triggering of the 1 April 2014 Mw 8.2 Iquique, Chile, earthquake, Earth and Planetary Science Letters, Volume 447, 1 August 2016, Pages 119-129, doi: 10.1016/j.epsl.2016.04.020, 2016.

Hitchmn, A.P, Lilley, F.E.M. and Campbell, W.H.: The quiet daily variation in the total magnetic field: global curves. Geophysical Research Letters, VOL. 25, NO. 11, p2007-2010, June 1, 1998, doi: 10.1029/98GL51332, 1998.

Hough, S. E.: Predicting the Unpredictable: The Tumultuous Science of Earthquake Prediction, Vol. 272, Princeton: Princeton University Press. doi: 10.1515/9781400883547, 2010.

Q. Huang: Rethinking earthquake-related DC-ULF electromagnetic phenomena: to- wards a physics-based approach, Nat. Hazards Earth Syst. Sci. 11 (2011), 2941– 2949, DOI: 10.5194/nhess-11-2941-2011

Ippolito, A., Perrone. L., De Santis, A. and Sabbagh D.: Ionosonde Data Analysis in Relation to the 2016 Central Italian Earthquakes. Geosciences 2020, 10, 354; doi:10.3390/geosciences10090354, 2020.

Jordan, T., Chen, Y., Gasparini, P., Madariaga, R., Main, I., Marzocchi, W., Papadopoulos, G., Sobolev, G., Yamaoka, K. and Zschau, J.: Operational earthquake forecasting. State of Knowledge and Guidelines for Utilization. Annals of Geophysics, 54(4), doi: 10.4401/ag-5350, 2011.

Kanamori, H.: The Energy Release in Great Earthquakes, J. Geophys. Res., 82(20), 2981–2987, doi: 10.1029/JB082i020p02981, 1977.

Karakeliana, D., Klemperera, S. L., Fraser-Smith, A. C., and Thompson, G. A.: Ultra-low frequency electromagnetic measurements associated with the 1998 Mw 5.1 San Juan Bautista, California earthquake

and implications for mechanisms of electromagnetic earthquake precursors, Tectonophysics, 359, 65–79, doi: 10.1016/S0040-1951(02)00439-0, 2002.

Kivelson, M, G. and Russell, C.T.: Introduction to Space Physics. Cambridge, Cambridge University Press, doi: 10.1017/9781139878296, 1995.

Kulsrud, R.: Plasma Physics for Astrophysics. Princeton University Press, U.S.A. Lanza, R., Meloni, A., 2004. The Earth's Magnetism – An Introduction for Geologists. Springer, Würzburg.

Lassak, T., McNamara, A., Garnero, E., and Zhong, S.: Core–mantle boundary topography as a possible constraint on lower mantle chemistry and dynamics. Earth and Planetary Science Letters, Vol. 289, Issues 1–2, 15 January 2010, Pages 232-241, doi: 10.1016/j.epsl.2009.11.012, 2010.

Lazarian, A., Eyink, G.L., Jafari, A., Kowal, G., Li, H., Xu, S. and Vishniac, E.T.: 3D turbulent reconnection: Theory, tests, and astrophysical implications. Physics of Plasmas 27, 012305 (2020); doi:10.1063/1.5110603, 2020.

Li, Z., Zhang, X., Wei, Y. and Ali, M.: Experimental Study of Electric Potential Response Characteristics of Different Lithological Samples Subject to Uniaxial Loading. Rock Mech Rock Eng (2020), doi:10.1007/s00603-020-02276-z, 2020.

Liu, J.Y.: Earthquake precursors observed in the ionospheric F-region. In Electromagnetic Phenomena Associated with Earthquakes (ed. Hayakawa, M.). Transworld Research Network, Trivandrum, India, pp. 187–204, 2009.

Ma, L., Zhao, J., and Ni, B.: A Zener-Stroh crack interacting with an edge dislocation, Theoretical and Applied Mechanics Letters, 2, 021003, doi:10.1063/2.1102103, 2011.

Marchetti, D. and Akhoondzadeh, M.: Analysis of Swarm satellites data showing seismo-ionospheric anomalies around the time of the strong Mexico (Mw = 8.2) earthquake of 08 September 2017. Advances in Space Research, Vol. 62, Issue 3, 1 August 2018, Pages 614-623, doi: 10.1016/j.asr.2018.04.043, 2018.

Marchetti, D., De Santis, A., D'Arcangelo, S., Poggio, F., Piscini, A., Campuzano, S.A. and De Carvalho, W.V.J.O.: Pre-earthquake chain processes detected from ground to satellite altitude in preparation of the 2016–2017 seismic sequence in Central Italy. Remote Sensing of Environment. Volume 229, August 2019, Pages 93-99, doi: 10.1016/j.rse.2019.04.033, 2019a.

Marchetti, D., Santis, A. D., Shen, X., Campuzano, S. A., Perrone, L., Piscini, A., Di Giovambattista, R., Jin, S., Ippolito, A., Cianchini, G., Cesaroni C., Sabbagh, D., Spogli, L. Zhima, Z. and Huang, J.: Possible Lithosphere-Atmosphere-Ionosphere Coupling effects prior to the 2018 Mw=7.5 Indonesia earthquake from seismic, atmospheric and ionospheric data. Journal of Asian Earth Sciences, 104097. doi: 10.1016/j.jseaes.2019.104097, 2019b.

McBeck, J.A., Zhu, W. and Renard, F.: The competition between fracture nucleation, propagation, and coalescence in dry and water-saturated crystalline rock. Solid Earth, 12, 375–387 (2021), doi: 10.5194/se-12-375-2021, 2021.

McFadden, P.L. and Merrill, R.T.: Geomagnetic Field, Asymmetries, Encyclopedia of Geomagnetism and Paleomagnetism, Edited by D. Gubbins and E. Herrero-Berbera. Springer, Netherlands, 2007.

Molchanov, O.A. and Hayakawa, M.: Seismo Electromagnetics and Related Phenomena: History and Latest Results. TERRAPUB, Tokyo, 2008.

Moldwin, M.: An introduction to space weather. Cambridge University Press. doi: 10.1017/CBO9780511801365, 2008.

Musson, R: Predicting the Unpredictable: The Tumultuous Science of Earthquake Prediction", Physics Today 63, 46-47 (2010), doi:10.1063/1.3518213, 2010.

Oikonomou, C., Haralambous, H. and Muslim, B.: Investigation of ionospheric precursors related to deep and intermediate earthquakes based on spectral and statistical analysis. Advances in Space Research 59 (2017) 587–602, doi: 10.1016/j.asr.2016.10.026, 2017.

Olson, P., Christensen, U.R. and Glatzmaier, G.A.: Numerical modeling of the geodynamo: mechanisms of field generation and equilibration, J. geophys. Res., 104, 10 383–10 404, doi: 10.1029/1999JB900013, 1999.

Olson, P.: Core Dynamics: An Introduction and Overview, Treatise on Geophysics (Second Edition) 2015, Pages 1–25 Reference Module in Earth Systems and Environmental Sciences Volume 8: Core Dynamics doi:10.1016/B978-0-444-53802-4.00137-8, 2015.

Oppenheim, A.V., Schafer, R.W., and Buck, J. R.: Discrete-Time Signal Processing. 2nd Ed. Upper Saddle River, NJ: Prentice Hall, 1999.

Park, J., Song, T.-R. A., Tromp, J., Okal, E., Stein, S., Roult, G., Clevede, E., Laske, G., Kanamori, H., Davis, P., Berger, J., Braitenberg, C., Van Camp, M., Lei, X., Sun, H., Xu, H. and Rosat, S.: Earth's Free Oscillations Excited by the 26 December 2004 Sumatra-Andaman Earthquake. Science 20 May 2005: Vol. 308, Issue 5725, pp. 1139-1144. doi: 10.1126/science.1112305, 2005.

Pasiou, E.D. and Triantis, D.: Correlation between the electric and acoustic signals emitted during compression of brittle materials, Frattura ed Integrità Strutturale, 40 (2017) 41-51, doi: 10.3221/IGF-ESIS.40.04, 2017.

Pedrera, A., Galindo-Zaldívar, J., Ruiz-Constán, A., Bohoyo, F., Torres-Carbonell, P., Ruano, P., Maestro, A. and González-Castillo, L.: The last major earthquakes along the Magallanes-Fagnano fault system recorded by disturbed trees (Tierra del Fuego, South America). Terra Nova 26, 448–453, doi: 10.1111/ter.12119, 2014.

Pomerantz, M.A.: Cosmic Rays. Published by The Commission on College Physics. Rd. Van Nostrand Reinhold Company, 1971.

Potirakis, S., Eftaxias, K., Schekotov, A., Yamaguchi, H. and Hayakawa, M.: Criticality features in ultra-low frequency magnetic fields prior to the 2013 M6.3 Kobe earthquake. Ann. Geophys. Vol. 59, No 3, doi: 10.4401/ag-6863, 2016.

Potirakis, S.M., Asano, T. and Hayakawa, M.: Criticality Analysis of the Lower Ionosphere Perturbations Prior to the 2016 Kumamoto (Japan) Earthquakes as Based on VLF Electromagnetic Wave Propagation Data Observed at Multiple Stations. Entropy 20, 199 (2018); doi: 10.3390/e20030199, 2018.

Priest, E.R., Forbes, T.: Magnetic Reconnection: Mhd Theory and Applications, Cambridge University Press, New York, 2000.

Prutkin, I.: Gravitational and magnetic models of the core–mantle boundary and their correlation. Journal of Geodynamics, Vol 45, Issues 2–3, March 2008, Pages 146-153, doi: 10.1016/j.jog.2007.09.001, 2008.

Pulinets, S. and Boyarchuk, K: Ionospheric Precursors of Earthquakes. Springer, Berlin, doi: 10.1007/b137616, 2004.

Pulinets, S.A., Davidenko, D.V. and Budnikov, P.A.: Method for Cognitive Identification of Ionospheric Precursors of Earthquakes. Geomagn. Aeron. 61, 14–24 (2021), doi:10.1134/S0016793221010126, 2021.

Rabiner, L.R. and Schafer, R.W.: Digital Processing of Speech Signals. The Journal of the Acoustical Society of America 67, 1406 (1980); doi: 10.1121/1.384160, 1980.

Russel, C.T., Zhou, X.W., Chi, P.J., Kawano, H., Moore, T.E., Peterson, W.K., Cladis, J.B. and Singer, H.J.: Sudden compression of the outer magnetosphere associated with an ionospheric mass ejection. Geophys. Res. Lett. 26,2343, doi:10.1029/1999GL900455, 1999.

Saltiel, S., Bonner, B.P., Mittal, T., Delbridge, B., and Ajo-Frankl, J.B.: Experimental evidence for dynamic friction on rock fractures from frequency-dependent nonlinear hysteresis and harmonic generation, J. Geophys. Res. Solid Earth, 122,4982–4999 (2017), doi:10.1002/2017JB014219, 2017.

Sarlis, N.V., Christopoulos, S.-R.G., and Skordas, E.S.: Minima of the fluctuations of the order parameter of global seismicity", Chaos 25 (2015), 063110, doi: 10.1063/1.4922300, 2015.

Sarlis, N.V., Skordas, E.S., Varotsos, P.A., Ramirez-Rojas, A., and Flores-Marquez E. L.: Identifying the Occurrence Time of the Deadly Mexico M8.2 Earthquake on 7 September 2017, Entropy, 21 (2019), 301, doi: 10.3390/e21030301, 2019.

Sarson, G.R.: Dynamo Waves, Encyclopedia of Geomagnetism and Paleomagnetism, Edited by D. Gubbins and E. Herrero-Berbera. Springer, Netherlands, 2007.

Satake, K., Heidarzadeh, M., Quiroz, M. and Cienfuegos, R.: History and features of trans-oceanic tsunamis and implications for paleo-tsunami studies. Earth-Science Reviews, Volume 202, March 2020, 103112, doi: 10.1016/j.earscirev.2020.103112, 2020.

Scoville, J., Heraud, J. and Freund, F.: Pre-earthquake magnetic pulses. Nat. Hazards Earth Syst. Sci., 15, 1873–1880, 2015. doi:10.5194/nhess-15-1873-2015, 2015.

Shea, M.A. and Smart, D.F.: Vertical cutoff rigidities for cosmic ray stations since 1955. Proc. 27th Int. Cosmic Ray Conf., Hamburg, 10, 4063–4066, 2001.

Scholz, C. H.: The Mechanics of Earthquakes and Faulting. 2nd edition. Cambridge University Press. ISBN 978-0-521-65540-8, 2002.

Selvadurai, P. A.: Laboratory insight into seismic estimates of energy partitioning during dynamic rupture: An observable scaling breakdown. Journal of Geophysical Research: Solid Earth. doi:10.1029/2018jb017194, 2019.

Silva, R. P., Sobral, J. H. A., Koga, D., and Souza, J. R.: Evidence of prompt penetration electric fields during HILDCAA events, Ann. Geophys., 35, 1165–1176, doi:10.5194/angeo-35-1165-2017, 2017.

Simmons, N.A., Forte, A.M., Boschi, L. and Grand, S.P.: Gypsum: A joint tomographic model of mantle density and seismic wave speeds. Journal of Geophysical Research (2010) 115: B12310. doi:10.1029/2010JB007631, 2010.

Slifkin, L.: Seismic electric signals from displacement of charged dislocations, Tectonophysics, 224, 149-152, doi:10.1016/0040-1951(93)90066-S,1993.

Smart, D.F., Shea, M.A., Flückiger, E.O.: Magnetospheric models and trajectory computations. Space Sci. Rev. 93 (1), 305–333, doi: 10.1023/A:1026556831199, 2000.

Smart, D.F., Shea, M.A.: Geomagnetic Cutoff Rigidity computer program Theory, Software Description and Example. Final Report, Grant NAG5-8009. Center for Space Plasmas and Aeronomic Research, the University of Alabama in Huntsville, 2001.

Smart, D.F. and Shea, M.A.: A review of geomagnetic cutoff rigidities for earth-orbiting spacecraft. Advances in Space Research 36 (2005) pp. 2012–2020. doi: 10.1016/j.asr.2004.09.015, 2005.

Soldati, G., Boschi, L., and Forte, A.M.: Tomography of core–mantle boundary and lowermost mantle coupled by geodynamics. Geophysical Journal International (2012) 189: 730–746, doi: 10.1111/j.1365-246X.2012.05413.x, 2012.

Soloviev, A., Chulliat, A., Bogoutdinov, S., Gvishiani, A., Agayan, S., Peltier, A. and Heumez, B.: Automated recognition of spikes in 1 Hz data recorded at the Easter Island magnetic observatory. Earth Planets Space, 64, 743–752, doi: 10.5047/eps.2012.03.004, 2012.

Stavrakas, I., Triantis, D., Agioutantis, Z., Maurigiannakis, S., Saltas, V., Vallianatos, F., and Clarke, M.: Pressure stimulated currents in rocks and their correlation with mechanical properties, Nat. Hazards Earth Syst. Sci., 4, 563–567, doi:10.5194/nhess-4-563-2004, 2004.

Stavrakas, I., Kourkoulis, S., and Triantis, D.: Damage evolution in marble under uniaxial compression monitored by Pressure Stimulated Currents and Acoustic Emissions. Frattura Ed Integrità Strutturale, 13(50), 573-583, doi:10.3221/IGF-ESIS.50.48, 2019.

Stewart, D.N., Busse, F.H., Whaler, K. and Gubbins, D.: Geomagnetism Earth rotation and the electrical conductivity of the lower mantle. Phys. Earth Planet. Inter., 92, 199-214), doi: 10.1016/0031-9201(95)03035-4, 1995.

Storini, M., Shea, M.A., Smart, D.F. and Cordaro, E.G.: Cutoff Variability for the Antarctic Laboratory for Cosmic Rays (LARC: 1955-1995). 26th International Cosmic Ray Conference. SH.3.6.30 .7 1999. 402, 1999.

Stroh, A. N.: The Formation of Cracks in Plastic Flow II, Philos. T. R. Soc. Lond., A232, 548–560, doi: 10.1098/rspa.1954.0124, 1955.

Sun, S.: Seismic velocities, anisotropy and elastic properties of crystalline rocks and implications for interpretation of seismic data (PhD thesis, École Polytechnique de Montréal). Retrieved from https://publications.polymtl.ca/725/, 2011.

Tarduno, J.A., Watkeys, M.K., Huffman, T.N., Cottrell, R.D., Blackman, E.G., Wendt, A., Scribner, C.A. and Wagner, C.L.: Antiquity of the South Atlantic Anomaly and evidence for top-down control on the geodynamo. Nat Commun 6, 7865, doi:10.1038/ncomms8865, 2015.

Telesca L., Lapenna V., Alexis N., Multiresolution wavelet analysis of earthquakes, Chaos, Solitons & Fractals 22, 741 (2004).

Telesca L., Hloupis G., Nikolintaga I., Vallianatos F., Temporal patterns in southern Aegean seismicity revealed by the multiresolution wavelet analysis, Communications in Nonlinear Science and Numerical Simulation 12, 1418 (2007).

Torrence, C. and Compo, G.P.: A Practical Guide to Wavelet Analysis. Bulletin of the American Meteorological Society, vol. 79, Issue 1, pp.61-78, doi: 10.1175/1520-0477(1998)079<0061:APGTWA>2.0.CO;2, 1998.

Triantis, D., Anastasiadis, C. and Stavrakas, I.: The correlation of electrical charge with strain on stressed rock samples, Nat. Hazards Earth Syst. Sci., 8, 1243–1248, doi:10.5194/nhess-8-1243-2008, 2008.

Triantis D., Vallianatos F., Stavrakas I. and Hloupis G.: Relaxation phenomena of electrical signal emissions from rock following application of abrupt mechanical stress. Annals of Geophysics, 55, 1, 2012; doi:10.4401/ag-5316, 2012.

Triantis, D., Stavrakas, I., Kyriazopoulos A., Pasiou E.D. and Kourkoulis, S.K.: Monitoring the mechanical response of early aged cement-mortar specimens using the Pressure Stimulated Currents technique. Procedia Structural Integrity, Vol. 28, 2020, Pages 502-510, doi: 10.1016/j.prostr.2020.10.059, 2020.

Tsyganenko, N.A.: A model of the near magnetosphere with a dawn-dusk asymmetry 1. Mathematical structure. J. Geophys. Res. 107 (A8), 1179, doi: 10.1029/2001JA000219, SMP12-1-17, 2002a.

Tsyganenko, N.A.: A model of the near magnetosphere with a dawn-dusk asymmetry 2: parametrization and fitting to observation. J. Geophys. Res. 107 (A8), 1176, doi:10.1029/2001JA000219, 2002b.

Tzanis, A. and Vallianatos, F.: A physical model of electrical earthquake precursors due to crack propagation and the motion of charged edge dislocations. Seismo Electromagnetics (Lithosphere–Atmosphere–Ionosphere-Coupling), TerraPub, 2002, pp. 117–130, 2002.

Utada, H., Shimizu, H., Ogawa, T., Maeda, T., Furumura, T., Yamamoto, T., Yamazaki, N., Yoshitake, Y., and Nagamachi, S.: Geomagnetic field changes in response to the 2011 off the Pacific Coast of Tohoku earthquake and tsunami, Earth Planet. Sc. Lett., 311, 11–27, doi: 10.1016/j.epsl.2011.09.036, 2011.

Vallianatos, F. and Tzanis, A.: On the nature, scaling and spectral properties of pre-seismic ULF signals. Natural Hazards and Earth System Sciences (2003) 3: 237–242. European Geosciences Union, doi: 10.5194/nhess-3-237-2003, 2003.

Varotsos, P. and Alexopoulos, K.: Physical properties of the variations of the electric field of the earth preceding earthquakes, I. Tectonophysics 110 (1984), 73-98, doi:10.1016/0040-1951(84)90059-3, 1984.

Varotsos, P., Eftaxias, K., Lazaridou, M., Antonopoulos, G., Makris, J. and Poliyiannakis, J.: Summary of the five principles suggested by Varotsos et al. [1996] and the additional questions raised in this debate. Geophysical Research Letter. Volume23, Issue 11, 27 May 1996, p1449-1452, doi: 10.1029/96GL01437, 1996.

Varotsos, P.A.: The Physics of Seismic Electric Signals. Journal of atmospheric electricity, 33(1), 53-68, TERRAPUB, Tokyo, 2005.

Varotsos, P.A., Sarlis, N.V. and Skordas, E.S.: Phenomena preceding major earthquakes interconnected through a physical model, Annales Geophysicae 37 (2019), 315–324, doi: 10.5194/angeo-37-315-2019, 2019.

Venegas-Aravena, P., Cordaro E.G. and Laroze. D.: A review and upgrade of the lithospheric dynamics in context of the seismo-electromagnetic theory. Natural Hazards Earth System Sciences. 119, 1- 13, doi: 10.5194/nhess- 19-1-2019, 2019.

Venegas-Aravena, P., Cordaro E.G. and Laroze. D.: The spatial–temporal total friction coefficient of the fault viewed from the perspective of seismo-electromagnetic theory. Nat. Hazards Earth Syst. Sci., 20, 1485–1496, doi: 10.5194/nhess-20-1485-2020, 2020.

Vezzoli, L. and Acoocella, V.: Easter Island, SE Pacific: An end-member type of hotspot volcanism. Geological Society of American Bulletin, May/june 2009, V. 121; no 5/6, p 869-886, doi:10.1130/B26470.1, 2009.

Vigny, C., Socquet, A., Peyrat, S., Ruegg, J.-C., Metois, M., Madariaga, R., Morvan, S.,Lancieri, M., Lacassin, R., Campos, J., Carrizo, D., Bejar-Pizarro, M., Barrientos, S., Armijo, R., Aranda, C., Valderas-Bermejo, M.-C., Ortega, I., Bondoux, F., Baize, S.,Lyon-Caen, H., Pavez, A., Vilotte, J. P., Bevis, M., Brooks, B., Smalley, R., Parra, H., Baez, J.-C., Blanco, M., Cimbaro, S., and Kendrick, E.: The 2010 Mw 8.8 Maule Megathrust Earthquake of Central Chile, monitored by GPS, Science, 332, 1417–1421, doi: 10.1126/science.1204132, 2011.

Villalobos, C.U., Bravo, M.A., Ovalle, E.M. and Foppiano, A.J.: Ionospheric characteristics prior to the greatest earthquake in recorded history. Advances in Space Research, 57 (2016) 1345–1359, doi: 10.1016/j.asr.2015.09.015, 2016.

Vogel, E. E., Brevis, F. G., Pastén, D., Muñoz, V., Miranda, R. A., and Chian, A. C.-L.: Measuring the seismic risk along the Nazca–South American subduction front: Shannon entropy and mutability, Nat. Hazards Earth Syst. Sci., 20, 2943–2960, doi:10.5194/nhess-20-2943-2020, 2020.

Yamanaka, C., Matsumoto, H. and Asahara, H.: Preseismic Electromagnetic Phenomena. IEEJ Transactions on Fundamentals and Materials. Special Issue Paper, 2016 Volume 136 Issue 5 Pages 310-314, doi: 10.1541/ieejfms.136.310, 2016.

Yeeram, T.: The solar wind-magnetosphere coupling and daytime disturbance electric fields in equatorial ionosphere during consecutive recurrent geomagnetic storms. Journal of Atmospheric and Solar-Terrestrial Physics, Volume 187, June 2019, Pages 40-52, doi: 10.1016/j.jastp.2019.03.004, 2019.

Yoshida, M.: Core–mantle boundary topography estimated from numerical simulations of instantaneous mantle flow. Geochemistry, Geophysics, Geosystems, Vol. 9, No. 7, 2 July 2008, doi: 10.1029/2008GC002008, 2008.

Yu, Z., Hattori, K., Zhu, K., Fan, M., Marchetti, D., He, X. and Chi, C.: Evaluation of Pre-Earthquake Anomalies of Borehole Strain Network by Using Receiver Operating Characteristic Curve. Remote Sensing. 2021; 13(3):515, doi:10.3390/rs13030515, 2021.

Zhang, Y., Zhang, G., Hetland, E.A., Shan, X., Wen, S. and Zuo, R.: Coseismic Fault Slip of the September 16, 2015 Mw 8.3 Illapel, Chile Earthquake Estimated from InSAR Data. In: Braitenberg C., Rabinovich A. (eds) The Chile-2015 (Illapel) Earthquake and Tsunami. Pageoph Topical Volumes. Birkhäuser, Cham, doi: 10.1007/978-3-319-57822-4_7, 2017.

Zlotnicki, J., Kossobokov, V. and Le Mouel, J.-L.: Frequency spectral properties of an ULF electromagnetic signal around the 21 July 1995, M=5.7, Yong Deng (China) earthquake, Tectonophysics 334 (2001), 259-270, doi: 10.1016/S0040-1951(00)00222-5, 2001.

Figure Captions

Figure 1: Left side: Latitudinal effect of the Geomagnetic cutoff rigidity projected over the Chilean convergent margin close to the 70° W meridian. The pink solid lines indicate the edges of tectonic plates. Nazca Plate from 18° North to 45° degrees latitudinal, The South American Continent on the South American Plate. The 45 ° to 79° of the Antarctic Plate. The black lines indicate the coast line. In blue the iso values of magnetic intensity due SAMA proximity. The symbols indicate the station's location. Right: History of Chilean earthquakes.

Figure 2: The Kp magnetic activity index for the periods prior to the Maule 2010 (top), Iquique 2014 (middle) and Illapel 2015 (bottom) earthquakes. [spidr NOAA] [WDCFG Kyoto University] .

Figure 3: Vertical Component B_z as a function of time at Putre and IPM stations. a) Maule 2010 at the Putre station, b) Iquique 2014 at the Putre station, c) Iquique 2014 at the Easter Island station and d) Illapel 2015 at Easter island station. Trends changes have been observed in the four cases.

Figure 4: a) Fast Fourier Transformation (FFT) of the second derivative B_z component at Putre station for different events: Maule 2010 and Iquique 2014. The rise of frequencies in the range of micro Hz are compared to the FFT of the second derivative at IPM station for Illapel 2015. b) FFT every 15 days for Iquique 2015 at the Putre magnetometer. c) FFT every 8 days for Illapel 2015 at the Easter Island magnetometer.

Figure 5: Wavelet for Bz at OSO station is shown. This graph is obtained by restricting the peaks considered in a band and daily average values during 2 years of measurements. Wavelet spectrum shows an increase prior and after the Maule Earthquake. Unlike the spectrogram method where it is enough to consider the anomalous peaks on a threshold, wavelet analysis is more complex to calibrate than spectrogram analysis (upper limit).

Figure 6: Spectrograms analysis of vertical magnetic components after the external influence is filtered. a) The rise of a range of frequencies (1-2.5 mHz) appear prior and after the Maule 2010 earthquake (OSO station). The active frequencies last less than 3 months. b) The rise of similar frequencies appears prior to the Iquique 2014 earthquake in the vertical component of PIL station. This frequency activity lasts more than five months. c) The solar events were intense during September 2015. Nevertheless, it can be seen as an increase in the spectrum since August 2015. This frequency activity lasts close to 3 months. Three earthquakes hit when exist the rise of ultra-low frequencies (mHz)

Figure 7: Accumulated magnetic anomalies of B_z and a linear interpolation in the period during two years starting on 29 February 2009. The data were taken at OSO Station. Close to the Main earthquake, the linear trend breaks and the number of anomalies increase. Other important seismic events hit near the stations during the last period. Nevertheless, it is not clear that the anomaly increases are due these specific events.

Figure 8: Variation of the accumulated diary of magnetic anomalies of B_z during two years close to the three earthquakes: (a) Maule, (b) Iquique and (c) Illapel. The data were taken at OSO station (a) and PIL station (b & c), respectively. Is clear that the sigmoidal shape is similar in all of the earthquakes. This means that these stations recorded a dramatic increase in the number of magnetic anomalies between 50 to 90 days prior each earthquake.

Figure 9: (Upper panel) Accumulated Diary of magnetic anomalies during two years, in component Y from Apr 1 to Oct 15, 2017 in Mexico Earthquake Sep 8, 2017 Mw8.2. (Lower panel) Residual behavior of Mexico Earthquake. The data is open source and was taken from the swarm project (ftp://swarm-diss.eo.esa.int/). Methodology was developed by Marchetti and Akhoondzadeh (2018).

Figure 10: Schematic representation of the seimo-electromagnetic theory. The anomalies generation are owing the creation of several microcracks. The number of cracks increase because the internal collapse of the lithosphere when a non-constant uniaxial stress is applied.

Table Captions

Table 1: The main characteristics for the detector of Chilean network Cosmic Rays and Geomagnetic Observatories as location, altitude, and atmospheric depth, type of detectors (Cordaro et al., 2012).

Table 2: The maximum radius where the ionosphere-lithosphere-atmosphere coupling may affect magnetic measurements to each earthquake studied at the station of Putre and IPM. (Dobrovolsky et al., 1979, Pulinets and Boyarchuk, 2004). The Preparation area or Dobrovolsky area is defined by the radius $r = 10^{0.43M}$, where M is the earthquake magnitude. This table shows that Putre and IPM stations are within the earthquake preparation stage for Maule, Iquique and Illapel.

Table 3: Days before and after each frequency or anomalies rises for each considered earthquakes (Maule 2010, Iquique 2014, Illapel 2015 and Mexico 2017 for anomalies).

FIGURES

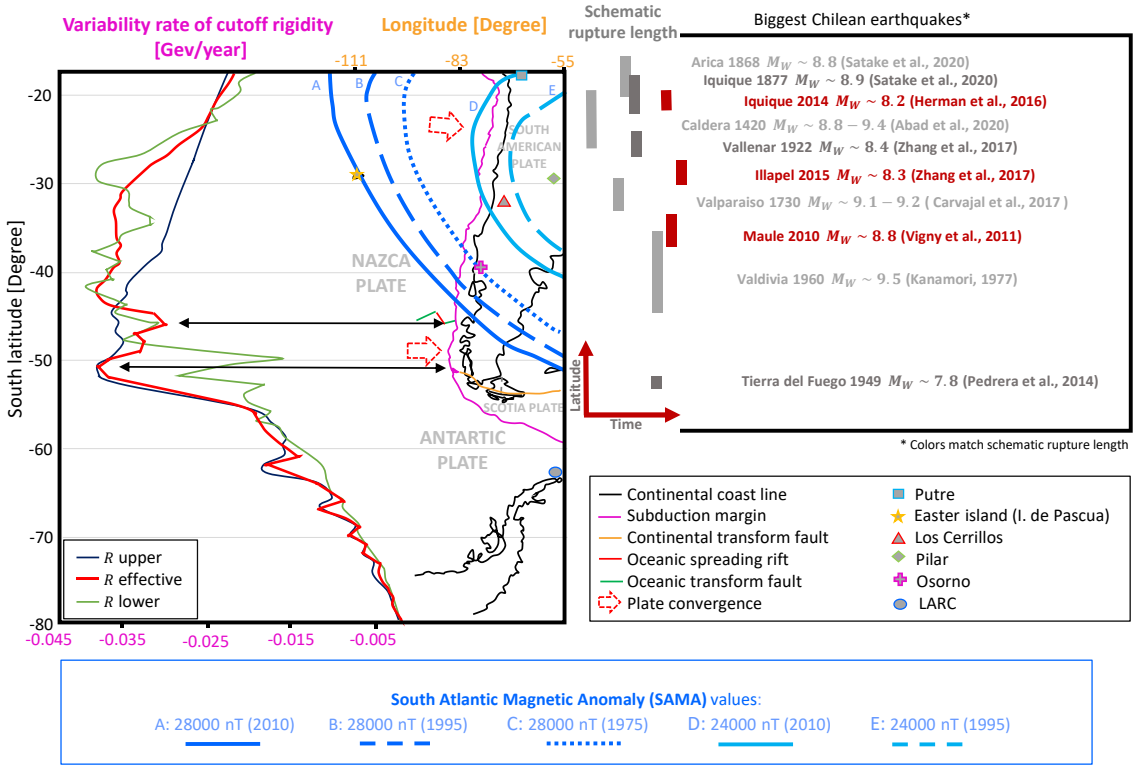

Figure 1

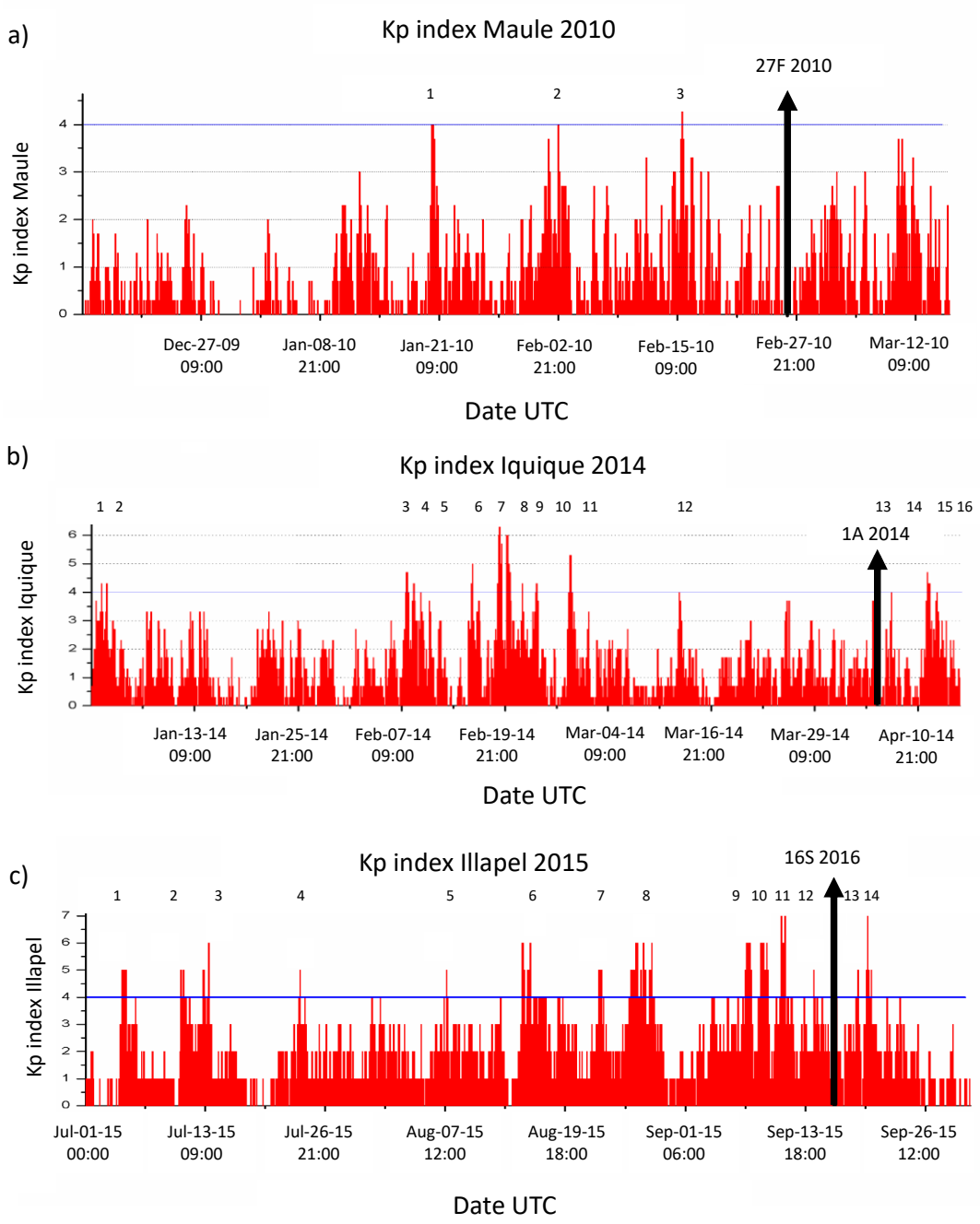
a)
Kp index Maule 2010
27F 2010
1
2
3
Kp index Maule
0
1
2
3
4
Dec-27-09 09:00
Jan-08-10 21:00
Jan-21-10 09:00
Feb-02-10 21:00
Feb-15-10 09:00
Feb-27-10 21:00
Mar-12-10 09:00
Date UTC
b)
Kp index Iquique 2014
1 2
3 4 5
6 7 8 9 10 11
12
13 14 15 16
1A 2014
Kp index Iquique
0
1
2
3
4
5
6
Jan-13-14 09:00
Jan-25-14 21:00
Feb-07-14 09:00
Feb-19-14 21:00
Mar-04-14 09:00
Mar-16-14 21:00
Mar-29-14 09:00
Apr-10-14 21:00
Date UTC
c)
Kp index Illapel 2015
16S 2016
1
2
3
4
5
6
7
8
9 10 11 12
13 14
Kp index Illapel
0
1
2
3
4
5
6
7
Jul-01-15 00:00
Jul-13-15 09:00
Jul-26-15 21:00
Aug-07-15 12:00
Aug-19-15 18:00
Sep-01-15 06:00
Sep-13-15 18:00
Sep-26-15 12:00
Date UTC

Figure 2 a,b,c

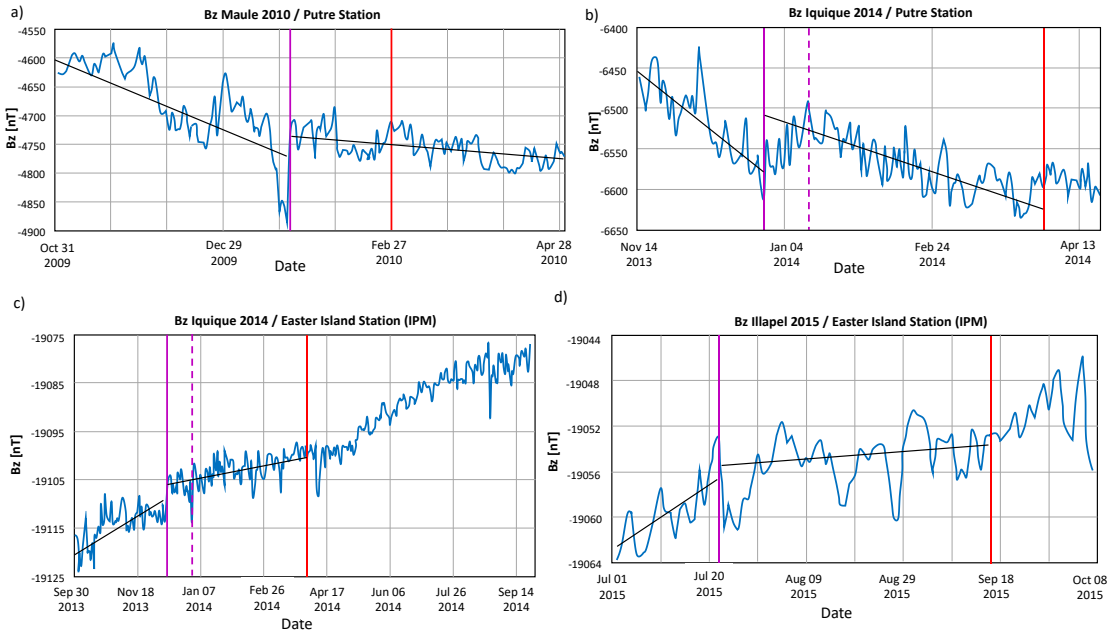

Figure 3 a, b, c, d

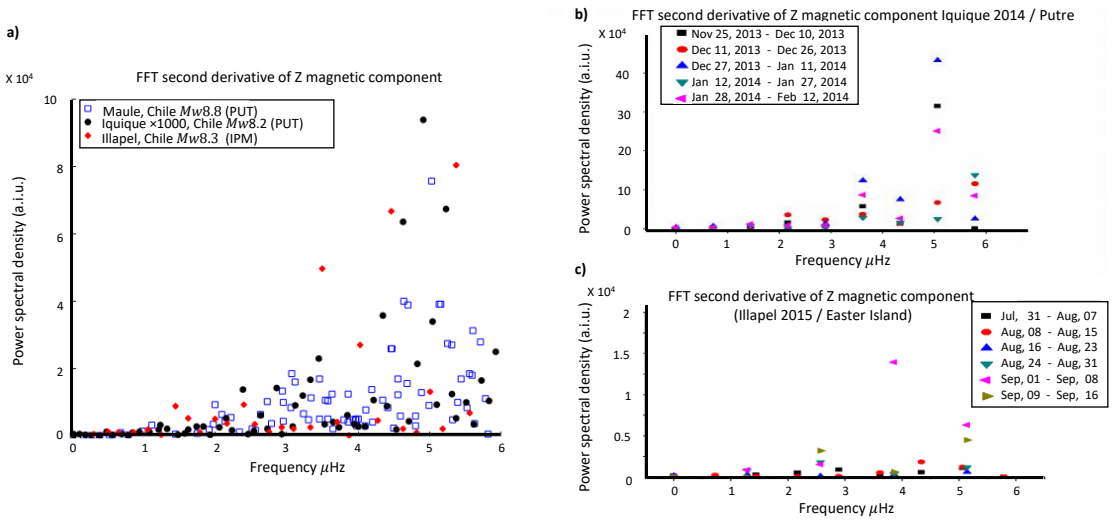
a)
FFT second derivative of Z magnetic component
X 10⁴
Maule, Chile Mw8.8 (PUT)
Iquique ×1000, Chile Mw8.2 (PUT)
Illapel, Chile Mw8.3 (IPM)
Power spectral density (a.i.u.)
Frequency μHz
b)
FFT second derivative of Z magnetic component Iquique 2014 / Putre
X 10⁴
Nov 25, 2013 - Dec 10, 2013
Dec 11, 2013 - Dec 26, 2013
Dec 27, 2013 - Jan 11, 2014
Jan 12, 2014 - Jan 27, 2014
Jan 28, 2014 - Feb 12, 2014
Power spectral density (a.i.u.)
Frequency μHz
c)
FFT second derivative of Z magnetic component
(Illapel 2015 / Easter Island)
X 10⁴
Jul, 31 - Aug, 07
Aug, 08 - Aug, 15
Aug, 16 - Aug, 23
Aug, 24 - Aug, 31
Sep, 01 - Sep, 08
Sep, 09 - Sep, 16
Power spectral density (a.i.u.)
Frequency μHz

Figure 4 a,b,c

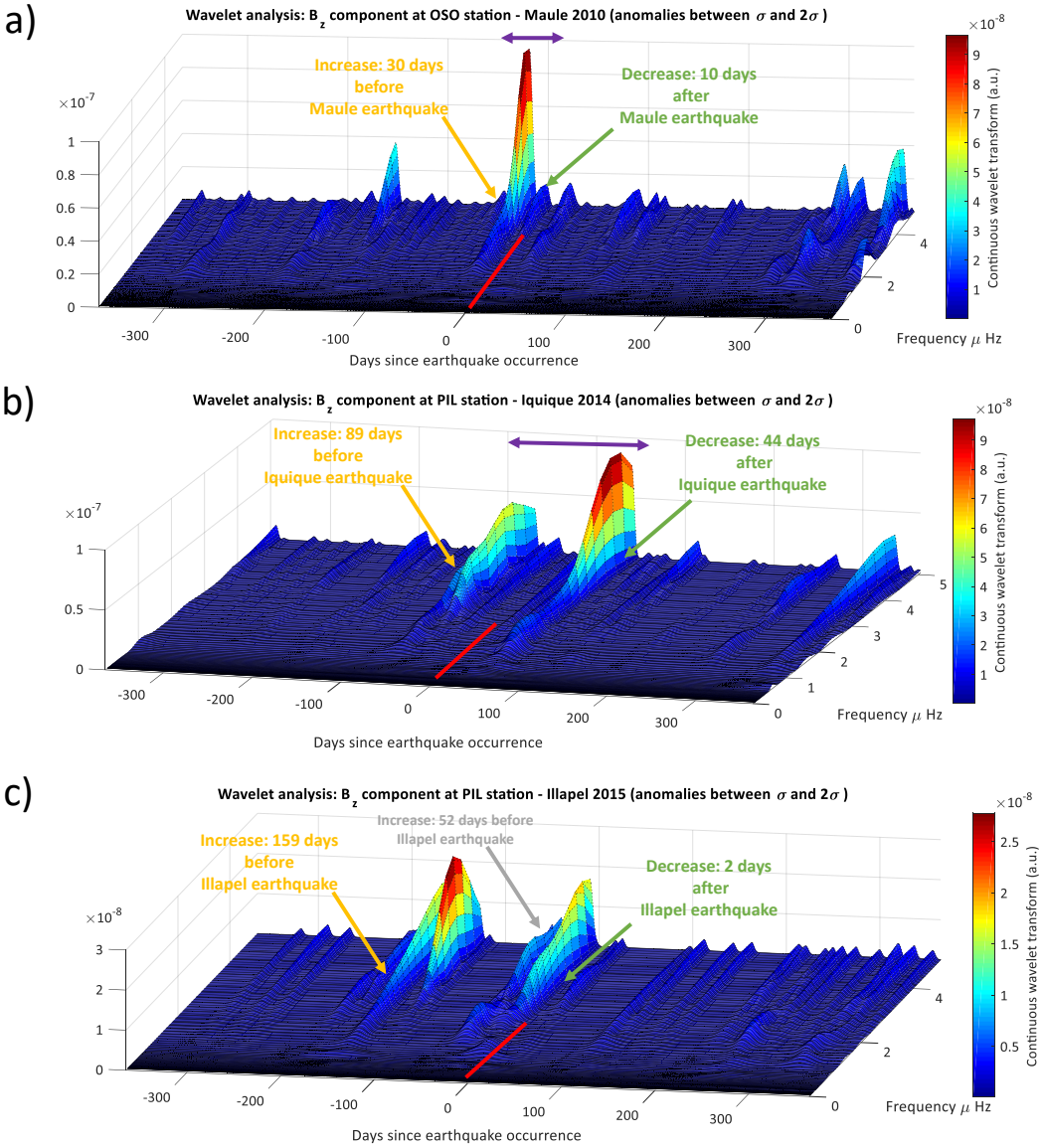
a)
Wavelet analysis: B_z component at OSO station - Maule 2010 (anomalies between σ and 2σ)
Increase: 30 days before Maule earthquake
Decrease: 10 days after Maule earthquake
Days since earthquake occurrence
Frequency μ Hz
Continuous wavelet transform (a.u.)
b)
Wavelet analysis: B_z component at PIL station - Iquique 2014 (anomalies between σ and 2σ)
Increase: 89 days before Iquique earthquake
Decrease: 44 days after Iquique earthquake
Days since earthquake occurrence
Frequency μ Hz
Continuous wavelet transform (a.u.)
c)
Wavelet analysis: B_z component at PIL station - Illapel 2015 (anomalies between σ and 2σ)
Increase: 159 days before Illapel earthquake
Increase: 52 days before Illapel earthquake
Decrease: 2 days after Illapel earthquake
Days since earthquake occurrence
Frequency μ Hz
Continuous wavelet transform (a.u.)

Figure 5

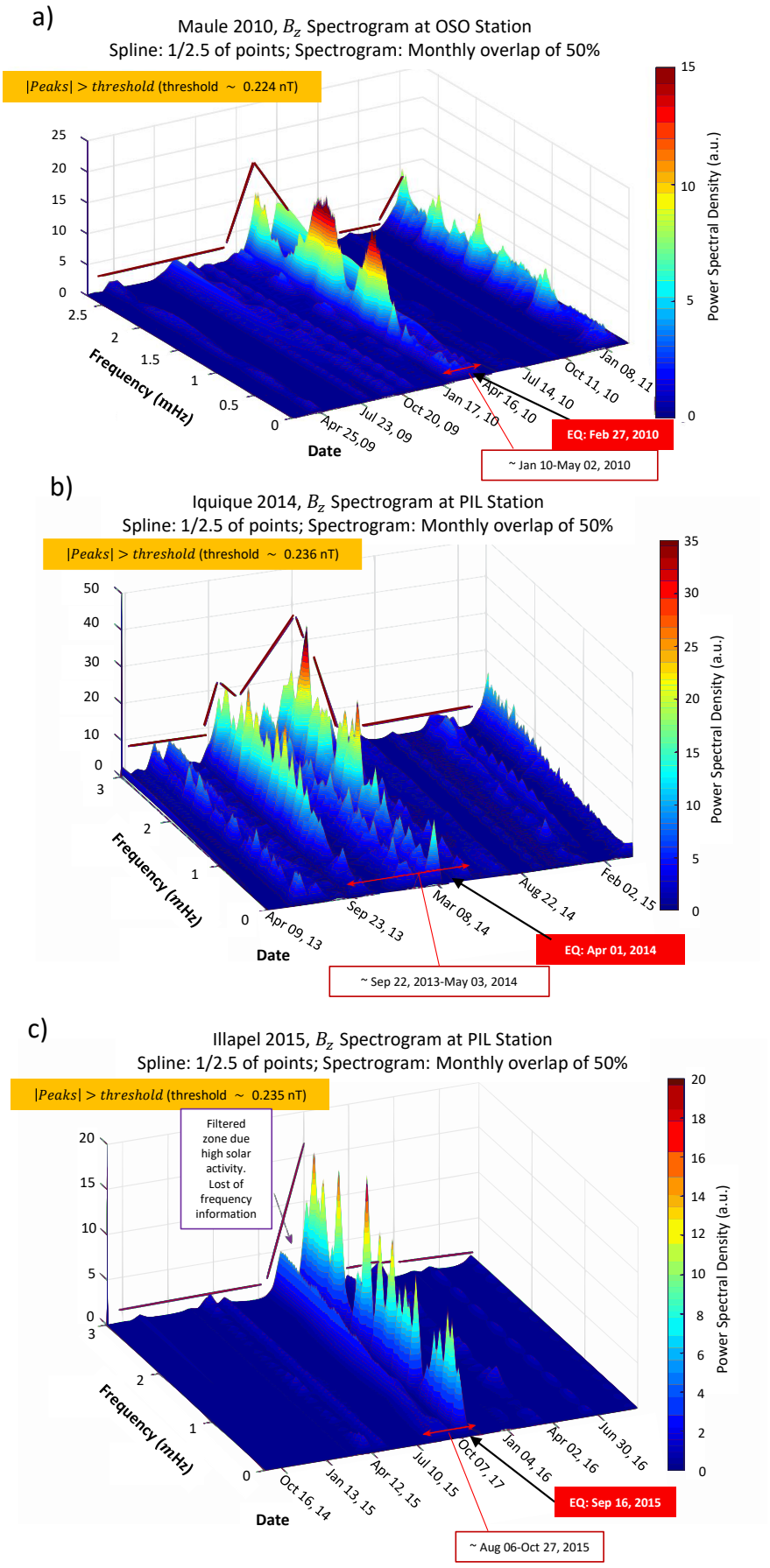
a)
Maule 2010, B_z Spectrogram at OSO Station
Spline: 1/2.5 of points; Spectrogram: Monthly overlap of 50%
$|Peaks| > threshold$ (threshold ~ 0.224 nT)
Frequency (mHz)
Date
Power Spectral Density (a.u.)
Apr 25,09
Jul 23, 09
Oct 20, 09
Jan 17, 10
Apr 16, 10
Jul 14, 10
Oct 11, 10
Jan 08, 11
EQ: Feb 27, 2010
~ Jan 10-May 02, 2010
b)
Iquique 2014, B_z Spectrogram at PIL Station
Spline: 1/2.5 of points; Spectrogram: Monthly overlap of 50%
$|Peaks| > threshold$ (threshold ~ 0.236 nT)
Frequency (mHz)
Date
Power Spectral Density (a.u.)
Apr 09, 13
Sep 23, 13
Mar 08, 14
Aug 22, 14
Feb 02, 15
EQ: Apr 01, 2014
~ Sep 22, 2013-May 03, 2014
c)
Illapel 2015, B_z Spectrogram at PIL Station
Spline: 1/2.5 of points; Spectrogram: Monthly overlap of 50%
$|Peaks| > threshold$ (threshold ~ 0.235 nT)
Filtered zone due high solar activity. Lost of frequency information
Frequency (mHz)
Date
Power Spectral Density (a.u.)
Oct 16, 14
Jan 13, 15
Apr 12, 15
Jul 10, 15
Oct 07, 17
Jan 04, 16
Apr 02, 16
Jun 30, 16
EQ: Sep 16, 2015
~ Aug 06-Oct 27, 2015

Figure 6

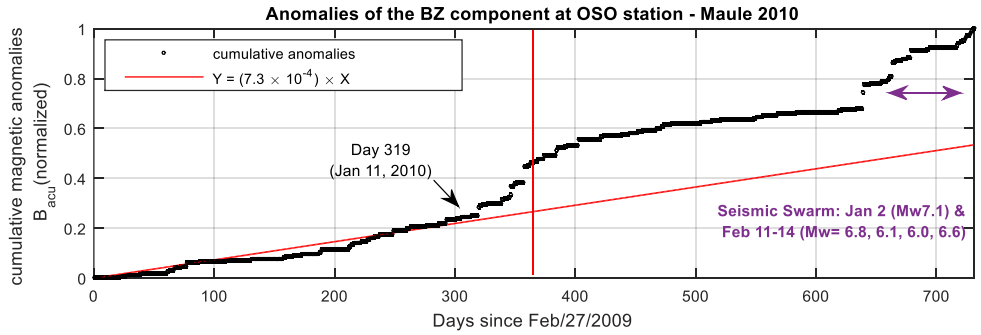
Anomalies of the BZ component at OSO station - Maule 2010
cumulative anomalies
Y = (7.3 × 10^-4) × X
Day 319
(Jan 11, 2010)
Seismic Swarm: Jan 2 (Mw7.1) &
Feb 11-14 (Mw= 6.8, 6.1, 6.0, 6.6)
cumulative magnetic anomalies
B_acu (normalized)
Days since Feb/27/2009
0
0.2
0.4
0.6
0.8
1
0
100
200
300
400
500
600
700

Figure 7

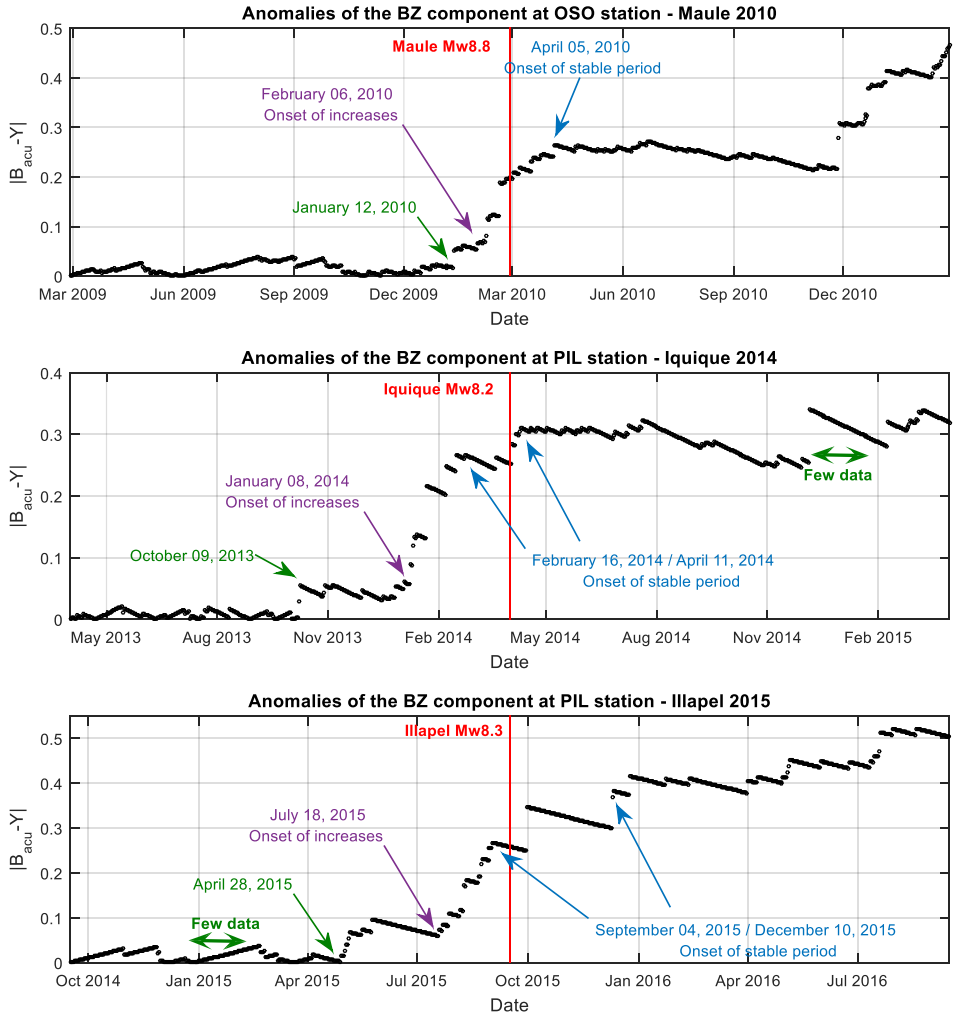
Anomalies of the BZ component at OSO station - Maule 2010
Maule Mw8.8
April 05, 2010
Onset of stable period
February 06, 2010
Onset of increases
January 12, 2010
|B_acu -Y|
Mar 2009
Jun 2009
Sep 2009
Dec 2009
Mar 2010
Jun 2010
Sep 2010
Dec 2010
Date
Anomalies of the BZ component at PIL station - Iquique 2014
Iquique Mw8.2
January 08, 2014
Onset of increases
October 09, 2013
Few data
February 16, 2014 / April 11, 2014
Onset of stable period
May 2013
Aug 2013
Nov 2013
Feb 2014
May 2014
Aug 2014
Nov 2014
Feb 2015
Anomalies of the BZ component at PIL station - Illapel 2015
Illapel Mw8.3
July 18, 2015
Onset of increases
April 28, 2015
Few data
September 04, 2015 / December 10, 2015
Onset of stable period
Oct 2014
Jan 2015
Apr 2015
Jul 2015
Oct 2015
Jan 2016
Apr 2016
Jul 2016

Figure 8

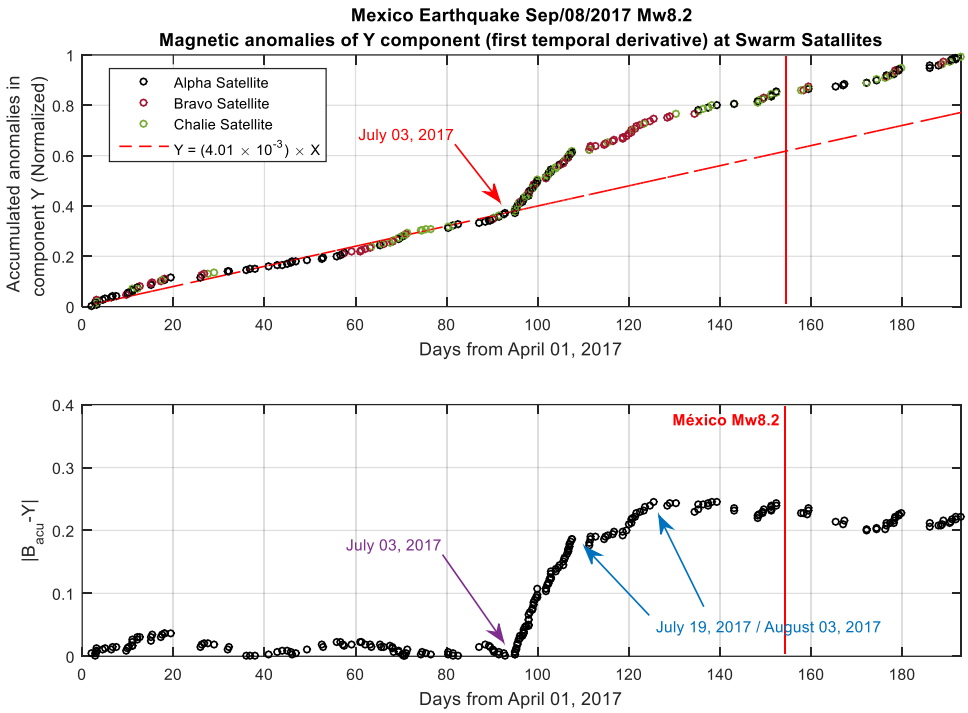
Mexico Earthquake Sep/08/2017 Mw8.2
Magnetic anomalies of Y component (first temporal derivative) at Swarm Satallites
Accumulated anomalies in component Y (Normalized)
Alpha Satellite
Bravo Satellite
Chalie Satellite
Y = (4.01 × 10^-3) × X
July 03, 2017
Days from April 01, 2017
|B_acu-Y|
México Mw8.2
July 03, 2017
July 19, 2017 / August 03, 2017
Days from April 01, 2017

Figure 9

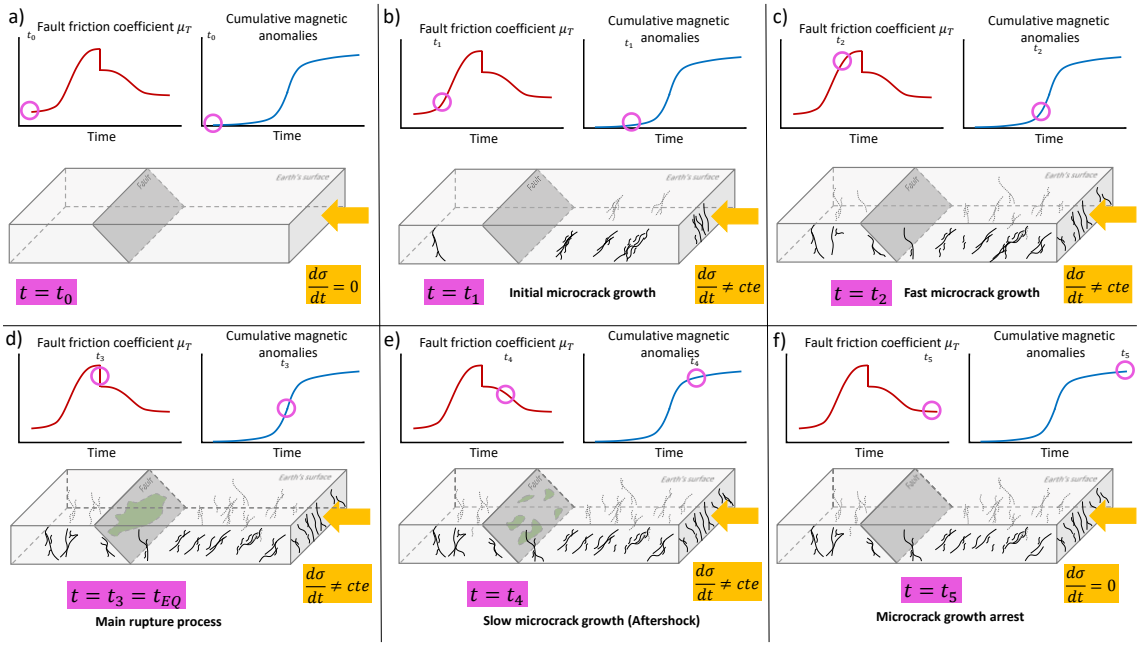
a)
Fault friction coefficient μ_T
t_0
Time
Cumulative magnetic anomalies
t_0
Time
Fault
Earth's surface
$t = t_0$
$\frac{d\sigma}{dt} = 0$
b)
Fault friction coefficient μ_T
t_1
Time
Cumulative magnetic anomalies
t_1
Time
Fault
Earth's surface
$t = t_1$
Initial microcrack growth
$\frac{d\sigma}{dt} \neq cte$
c)
Fault friction coefficient μ_T
t_2
Time
Cumulative magnetic anomalies
t_2
Time
Fault
Earth's surface
$t = t_2$
Fast microcrack growth
$\frac{d\sigma}{dt} \neq cte$
d)
Fault friction coefficient μ_T
t_3
Time
Cumulative magnetic anomalies
t_3
Time
Fault
Earth's surface
$t = t_3 = t_{EQ}$
Main rupture process
$\frac{d\sigma}{dt} \neq cte$
e)
Fault friction coefficient μ_T
t_4
Time
Cumulative magnetic anomalies
t_4
Time
Fault
Earth's surface
$t = t_4$
Slow microcrack growth (Aftershock)
$\frac{d\sigma}{dt} \neq cte$
f)
Fault friction coefficient μ_T
t_5
Time
Cumulative magnetic anomalies
t_5
Time
Fault
Earth's surface
$t = t_5$
Microcrack growth arrest
$\frac{d\sigma}{dt} = 0$

Figure 10

Observatory	Location	Geographical coordinate	Altitude [m.a.s.l]	Atmospheric Depth [g/cm2]	Instruments (Cordaro et al., 2012)	Time
PUTRE (PUT)	Andes Mountain, Chile	18°11´47.8 " S. 69°33´10.9" W	3.600	666	Magnetometer, UCLA-Vectorial-Flux Gate. Muon telescope, 3 channels. Neutron monitor IGY, 3 channels,He 3. UTC by GPS receiver.	2003-2017
Los Cerrillos (OLC)	Santiago de Chile, Chile	33°29´42.2" S. 70°42´59.81 W	570	955	Magnetometer, UCLA-Vectorial-Flux Gate. Multi-directional muon telescope, 7 channels. Neutron monitor 6NM64, 3 channels, BF-3. UTC by GPS receiver.	1958-2017
LARC	King George Island, Antarctic	62°12´9"S. 58°57´42¨ W	40	980	Magnetometer, UCLA-Vectorial-Flux Gate. Neutron monitor 6NM64 - BF-3BF-3. 6 channels. Neutron monitor 3NM64 – He-3. 3 channels, Neutron monitor 3NM64 – He-3.[Flux meter] 3 channels. UTC by GPS receiver.	1990-2017

Table 1

Event	Magnitude [Mw]	Radius r [km]	Station Distance from earthquake [km]
Maule 2010	8.8	~6100	Putre ~ 2030
Iquique 2014	8.2	~3360	Putre ~ 300
Illapel 2015	8.3	~3700	IPM ~ 3700

Table 2

Event	Rise of frequencies				Rise of cumulative anomalies, days before earthquake (secondary rise)
	Wavelet		Spectrogram		
	Days before earthquake (secondary rise)	Days after earthquake	Days before earthquake (secondary rise)	Days after earthquake	
Maule 2010	~30	~10	~48	~64	~46 (~21)
Iquique 2014	~89	~44	~191 (~95)	~32	~83
Illapel 2015	~159 (~52)	~2	~41	~41	~60
Mexico 2017	-	-	-	-	~67 (~42)

Table 3